

REVIEW ARTICLE

**Comparative planetary mineralogy: Valence state partitioning of Cr, Fe, Ti, and V among crystallographic sites in olivine, pyroxene, and spinel from planetary basalts**

J.J. PAPIKE\*, J.M. KARNER, AND C.K. SHEARER

Institute of Meteoritics, Department of Earth and Planetary Sciences, University of New Mexico, Albuquerque, New Mexico 87131-1126, U.S.A.

**ABSTRACT**

This is a comparative planetary mineralogy study emphasizing the valence-state partitioning of Cr, Fe, Ti, and V over crystallographic sites in olivine, pyroxene, and spinel from planetary basalts. The sites that accommodate these cations are the M2 site (6 to 8-coordinated) and M1 site (6-coordinated) in pyroxene, the M2 site (6- to 8-coordinated) and M1 (6-coordinated site) in olivine, and the tetrahedral and octahedral sites in spinel. The samples we studied are basalts from Earth, Moon, and Mars, and range in oxygen fugacity conditions from IW-2 (Moon) to IW+6 (Earth), with Mars somewhere in between (IW to IW+2). The significant elemental valence-states at these  $f_{O_2}$  conditions are (from low to high  $f_{O_2}$ ):  $Ti^{4+}$ ,  $V^{3+}$ ,  $Fe^{2+}$ ,  $Cr^{2+}$ ,  $Cr^{3+}$ ,  $V^{4+}$ , and  $Fe^{3+}$ .  $V^{2+}$  and  $Ti^{3+}$  play a minor role in the phases considered for the Moon, and are found in very low concentrations.  $V^{5+}$  plays a minor role in these phases in oxidized terrestrial basalts because it is probably lower in abundance than  $V^{4+}$ , and has an ionic radius that is so small (0.054 nm, 6-coordinated), that it is almost at the lower limit for octahedral coordination, and can even be tetrahedrally coordinated. The role of  $Cr^{2+}$  in the Moon is significant, as  $Cr^{2+}$  predominates in basaltic melts at  $f_{O_2}$  less than IW-1. Lunar olivine has been found to contain mostly  $Cr^{2+}$ , whereas coexisting pyroxene contains mostly  $Cr^{3+}$ .  $Fe^{3+}$  is very important in Earth, less so in Mars, and nonexistent in the Moon. The importance of the  $Fe^{2+}$  to  $Fe^{3+}$  transition cannot be overstated and, indeed, their crystal-chemical differences, in terms of behavior (based on size and charge), are similar to the differences between Mg and Al. We note that for pyroxene in six of the seven terrestrial suites we studied,  $Fe^{3+}$  (in the M1 site) coupled with Al (in the tetrahedral site) is one of the two most important charge-balance substitutions. This substitution is of lesser importance in Mars and does not exist in lunar basalts.

**INTRODUCTION**

This is a comparative planetary mineralogy study emphasizing the valence-state partitioning of Cr, Fe, Ti, and V over crystallographic sites in olivine, pyroxene, and spinel from planetary basalts. We concentrate on planetary basalts because basaltic volcanism is a fundamental process that has occurred on the Earth, Moon, Mars, and asteroids (especially 4 Vesta), from the beginning of the solar system at 4.56 Ga, to the present time. As partial melts of planetary interiors, basalts have compositions that are the product of many physical and chemical factors including the thermodynamic history of a planet, composition and mineralogy of the planet's interior, and post-extraction processes (e.g., Bence et al. 1980, 1981). Ultimately, many of these factors may be related to the origin and early evolution of the planetary body. Many studies have concentrated on the bulk-rock compositions of basalts to understand differences among basalt systems, and the influences of a planetary environment on a basalt system, in a comparative planetology context (Consolmagno and Drake 1977; Stolper 1979; Bence et al. 1980, 1981; Drake et al. 1989; Goodrich and Delaney 2000). This method works well when the basalts represent liquids erupted onto a planetary surface with little loss or gain of material (assimilation and/or cumulate processes).

A slight variation to the basalt bulk composition approach is to explore the compositions of the minerals in basalts, as they reflect the differing chemical and physical conditions of the melts from which they crystallized. Several studies have explored the composition of the silicate phases in planetary basalts to understand similarities and differences in a comparative context and/or to use individual minerals as petrogenetic and geochemical recorders (e.g., Bence and Papike 1972; Papike 1981, 1998). We have extended this philosophy to a set of comparative planetary mineralogy studies that combine major-, minor-, and trace-element data to correlate chemical trends in basaltic minerals with planetary origin and setting (e.g., Papike 1996; Papike et al. 1996). Our most recent studies (Karner et al. 2003, 2004b) reported the composition of olivine and plagioclase grains from 13 planetary basalt suites, relating the similarities and differences to the effects of igneous process, possible early solar system differentiation processes and planetary parentage. Studies, such as these, that concentrate on individual minerals in basalts are important because many present and future samples (Zolensky et al. 2000) of extraterrestrial planetary bodies are and will be from soils or regoliths, and may be too small to represent bulk-rock compositions. These "regolith" samples will have key information recorded in individual minerals, and this information can tell us not only about the source region of the rocks, but also

\* E-mail: jpapike@unm.edu

about the planetary body as a whole. In addition, many igneous samples are cumulates, and one particularly useful way to evaluate them is through the study of individual cumulate phases (Papike 1996).

This paper is written in review style and therefore starts with a summary of multivalent elements in basaltic melts, which is followed by a review of the crystal chemistry of olivine, pyroxene, and spinel. These crystal-chemistry reviews draw heavily from several prior works (Papike and Cameron 1976; Papike et al. 1976; Cameron and Papike 1980, 1981; Papike 1987). The remainder of the paper concentrates on the valence-state partitioning of Cr, Fe, Ti, and V into olivine, pyroxene, and spinel in basalts from the Earth, Moon and Mars. Major consideration for cation substitutions are ionic valence and radius (cf. Figs 1 and 2).

#### Variation in valence state in planetary basaltic melts

Over the range of  $f_{O_2}$  experienced by planetary basalts, [~Iron-Wustite (IW) -2 to IW+6] (e.g., Papike et al. 2004; Carmichael and Ghiorso 1990), cations such as Cr, Fe, Ti, and V exhibit a range of valence states that influence stability of mineral phases (e.g., Grove and Juster 1989), mineral compositions (e.g., McKay et al. 2004), and partitioning behavior between mineral and melt (e.g., Hanson and Jones 1998). At these  $f_{O_2}$  conditions, one would expect to find  $Fe^{3+, 2+}$ ,  $V^{5+, 4+, 3+, 2+}$ ,  $Cr^{3+, 2+}$  and  $Ti^{4+, 3+}$  in planetary basaltic melts (Fig. 1). Although Figure 1 shows the approximate point (in  $\log f_{O_2}$ ) at which the oxidized and reduced species of an element exist in equal proportions in a basaltic melt, it should be noted that the position of equilibrium redox boundaries will be modified by many factors. These factors include melt composition, melt structure, and electron-exchange reactions between multivalent elements within a melt.

Iron is the dominant multivalent cation in planetary basalts. In terrestrial and martian magmas, coupled reactions involving  $Fe^{2+}$

and  $Fe^{3+}$  influence the behavior of other minor to trace multivalent cations through electron-exchange reactions. Values of  $Fe^{3+}/Fe^{2+}$  have been shown to influence which minerals are on the liquidus and therefore the liquid line-of-descent for basaltic magmas. For example, Grove and Juster (1989) demonstrated that in basalts with relatively low  $Fe^{3+}/Fe^{2+}$  [near Quartz-Fayalite-Magnetite, (QFM)], pigeonite would be the dominant liquidus pyroxene, whereas at higher  $Fe^{3+}/Fe^{2+}$  (QFM+2), the higher  $MgO/FeO$  of the melt would promote the stability of orthopyroxene. Because  $Fe^{3+}$  and  $Fe^{2+}$  behave differently in a basaltic melt, the change in the  $Fe^{3+}/Fe^{2+}$  will also influence the melt structure, and hence viscosity as defined by the Non-Bridging Oxygens/Tetrahedral (NBO/T) ratio (Myers 1987). In lunar basalts, there is very little  $Fe^{3+}$ , whereas in terrestrial basalts, the  $Fe^{3+}/Fe^{2+}$  could be over 0.5.

In basaltic melts, V can potentially have valences of 2+, 3+, 4+, and 5+. In relatively oxidizing terrestrial environments,  $V^{4+}$  and  $V^{5+}$  are thought to dominate (Canil 1999). Using X-ray Absorption Near-Edge Structure (XANES) techniques, Sutton et al. (2005) and Karner et al. (2004a) determined the average V valence for several planetary basalt suites. Terrestrial basalt suites were dominated by  $V^{4+}$ : Hawaiian basalts showed a V valence range from 3.7 to 3.9; ocean floor basalts had an average V valence of 4.1; and melt inclusions from subduction zone basalts had an average V of 4.1. As expected, the V valence in lunar basalts was shown to be substantially lower; XANES measurements indicated that V in lunar basalts is dominated by  $V^{3+}$  with some evidence for  $V^{2+}$  (up to 20%).

In Fe-bearing basalts or Fe-bearing experimental melts above IW, it appears that most Cr is trivalent. However, in Fe-free systems at terrestrial  $f_{O_2}$  conditions, Cr occurs as both  $Cr^{3+}$  and  $Cr^{2+}$ . In addition, there is indirect evidence for divalent Cr in Fe-bearing systems from mineral-melt partitioning studies (e.g., Barnes 1986; Murck and Campbell 1986; Hanson and Jones 1998) and the high Cr content of some terrestrial olivine grains (Li et al. 1995). Berry et al. (2003) suggested that this discrepancy was a result of  $Cr^{2+}$  being oxidized to  $Cr^{3+}$  during cooling in the presence of  $Fe^{3+}$ , according to the electron-exchange reaction  $Cr^{2+} + Fe^{3+} \leftrightarrow Cr^{3+} + Fe^{2+}$ , and concluded that at terrestrial  $f_{O_2}$  conditions, approximately 50% of Cr in basaltic melts is divalent.

At  $f_{O_2}$  conditions below IW (where  $Fe^{3+}$  is rare) there appears

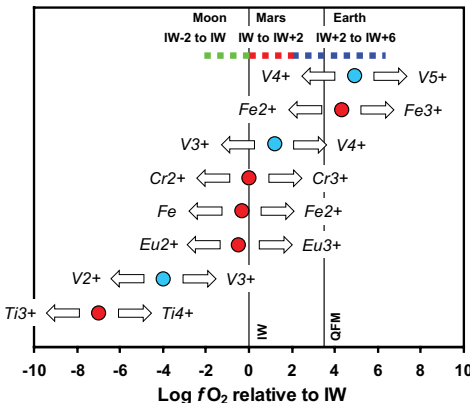


**FIGURE 1.** Schematic diagram of variable valence elements plotted at the  $f_{O_2}$  (relative to the IW buffer) where they occur. The circles represent the point (in  $\log f_{O_2}$ ) at which the oxidized and reduced species of an element exist in equal proportions in a basaltic melt. Note the great range in which V valences occur, covering over 8 orders of magnitude and spanning the  $f_{O_2}$  range of the solar system. The data used to construct this diagram are from Schreiber (1987) for Eu; Schreiber et al. (1987) for Fe; Hanson and Jones (1998) for Cr; Beckett (1986) for Ti; and Karner et al. (2004a), Sutton et al. (2002), and Canil (1999) for V. Diagram after Papike et al. (2004).

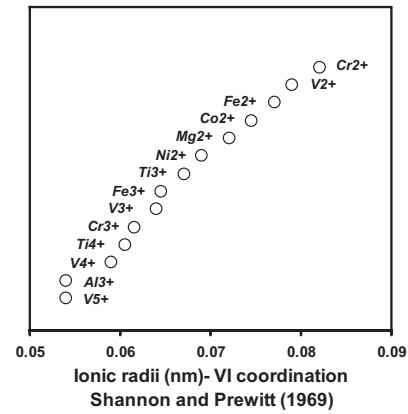


**FIGURE 2.** Ionic radii (nm) for octahedrally coordinated cations discussed in this paper.

to be a higher proportion of  $\text{Cr}^{2+}$ . For example, lunar mare basalts have a significantly larger concentration of Cr than basalts from Earth or Mars. Papike and Bence (1978) showed that  $\text{Cr}_2\text{O}_3$  in mare basalts varied between highs of 0.9 wt%  $\text{Cr}_2\text{O}_3$  at high Mg no. [=  $\text{Mg}/(\text{Mg} + \text{Fe})$  atomic] to 0.1 wt%  $\text{Cr}_2\text{O}_3$  at low Mg no. In comparison, MORB has concentrations below 0.2 wt%  $\text{Cr}_2\text{O}_3$ . Thus, Cr is markedly depleted in MORBs relative to mare basalts. Three possibilities for this depletion are: (1) all MORBs experienced early fractionation of Cr-spinel and/or Cr-spinel is an important residual phase in the source region; (2) the source regions for MORBs are depleted in Cr relative to mare source regions; (3) the low  $f_{\text{O}_2}$  on the Moon results in a significant reduction of  $\text{Cr}^{3+}$  to  $\text{Cr}^{2+}$  and this, in turn, affects the partition coefficients for mineral-melt equilibria, such that  $\text{Cr}^{2+}$  favors the melt relative to  $\text{Cr}^{3+}$  (Huebner et al. 1976; Schreiber and Haskin 1976; Delano 2001). Although all three of the above can play a role, we believe that (3) is the best explanation, based on the work of Hanson and Jones (1998). Direct evidence for significant  $\text{Cr}^{2+}$  in lunar melts has been documented by XANES of lunar pyroclastic glasses and experimental glasses produced below IW (S.R. Sutton 2004, personal communication).

At terrestrial and martian  $f_{\text{O}_2}$  conditions realized by basalts, Ti is tetravalent. Only in lunar basalts is there evidence for trivalent Ti. Indirect evidence for trivalent Ti in lunar basalts has been documented in pyroxene (Papike and Bence 1978; Papike and White 1979) and armalcolite (Papike et al. 1998). Burns et al. (1972) interpreted the absorption spectra of pyroxene grains to indicate some  $\text{Ti}^{3+}$ , while Schreiber (1977) calculated that 1 to 7% of the total lunar Ti was  $\text{Ti}^{3+}$ . XANES of lunar pyroclastic glasses indicates that the  $\text{Ti}^{3+}/(\text{Ti}^{3+} + \text{Ti}^{4+})$  in lunar basaltic magmas could be as high as 0.1 (S.R. Sutton 2004, personal communication).

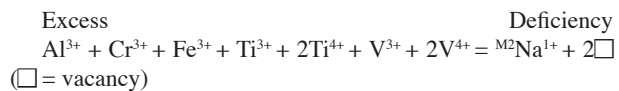
### Crystal chemistry of olivine

The compositions of the  $\text{Ca}-\text{Fe}^{2+}-\text{Mg}$  olivine grains can be represented on a quadrilateral (Fig. 3) with the end-members forsterite ( $\text{Mg}_2\text{SiO}_4$ ) fayalite ( $\text{Fe}^{2+}\text{SiO}_4$ ), monticellite ( $\text{CaMgSiO}_4$ ), and kirschsteinite ( $\text{CaFe}^{2+}\text{SiO}_4$ ). Complete solid solution occurs in the calcic series between monticellite and kirschsteinite and in the (Mg, Fe) series between forsterite and fayalite, but a miscibility gap exists between the two series at low temperatures. Other cations we consider include Cr, Ti, and V. Most naturally occurring olivine grains have compositions near the forsterite-fayalite series.

Olivine, at the relatively low pressures of the crust and upper mantle, crystallizes with orthorhombic space group symmetry  $Pbnm$ . Its structure approximates a closest-packed oxygen network with one half of the octahedral voids occupied by (Ca,  $\text{Fe}^{2+}$ , Mg) and one eighth of the tetrahedral voids occupied by Si. The structure can be visualized in terms of layers normal to the  $a$ -axis (Fig. 4). Individual layers consist of serrated chains of octahedra cross-linked by Si tetrahedra. Each layer is symmetrically identical to its neighbors but is displaced by a  $b/2$  glide. Extensive edge sharing causes strong distortions of the tetrahedra and octahedra. The M1 octahedron lies on a center of inversion, and its six shared edges are significantly shorter than the unshared edges. The M2 octahedron is located on a mirror plane, and its three shared edges are again shorter than the unshared edges. Distortion of the M1 and M2 octahedra increases

with substitution of the larger  $\text{Fe}^{2+}$  cation for Mg.

Olivine grains that plot in the quadrilateral are referred to as "Quad" (these include the divalent cations Ca, Mg, and  $\text{Fe}^{2+}$  and, for this paper, also include  $\text{Cr}^{2+}$  and  $\text{V}^{2+}$ ). Substitutions of  $\text{Cr}^{2+}$  or  $\text{V}^{2+}$  into the olivine crystal structure create no charge-balance problems. However, for cations with higher valences such as  $\text{Cr}^{3+}$ ,  $\text{Fe}^{3+}$ ,  $\text{Ti}^{3+}$ ,  $\text{Ti}^{4+}$ ,  $\text{V}^{3+}$ , and  $\text{V}^{4+}$  (we are not considering  $\text{V}^{5+}$  substitution into the olivine structure), we must have coupled substitutions to balance charge. Also,  $\text{Na}^{1+}$  in the olivine M2 site requires a coupled substitution. We call these cations "Others." All of the "others" cations will fit into the olivine crystal structure (Fig. 5). A simple way to express charge-balance Excess and Deficiency relative to "Quad" is as follows:



### Crystal chemistry of pyroxene

The general formula for a pyroxene can be written  $\text{XYZ}_2\text{O}_6$ , where X represents Na, Ca,  $\text{Mn}^{2+}$ ,  $\text{Fe}^{2+}$ , Mg, and Li in the M2 site; Y represents  $\text{Mn}^{2+}$ ,  $\text{Fe}^{2+}$ , Mg,  $\text{Fe}^{3+}$ , Al,  $\text{Cr}^{3+}$ , and  $\text{Ti}^{4+}$  in the M1 site; and Z represents Si and Al in the tetrahedral sites. Although Li and  $\text{Mn}^{2+}$  are important components in some pyroxene types (for example, spodumene,  $\text{LiAlSi}_2\text{O}_6$ , and johannsenite,  $\text{CaMn}^{2+}\text{Si}_2\text{O}_6$ ), they are trivial in most cases and are not considered here. Pyroxene compositions can be divided into two major groups, "Quad" and "Others." The former lie in a quadrilateral with end-members diopside (Di-  $\text{CaMgSi}_2\text{O}_6$ ), hedenbergite (Hed-  $\text{CaFe}^{2+}\text{Si}_2\text{O}_6$ ), enstatite (En-  $\text{Mg}_2\text{Si}_2\text{O}_6$ ) and ferrosillite (Fs-  $\text{Fe}^{2+}\text{Si}_2\text{O}_6$ ) (Fig. 6). For this paper we also consider  $\text{Cr}^{2+}$  and  $\text{V}^{2+}$  as "Quad" cations. Augite comprises solid solutions near

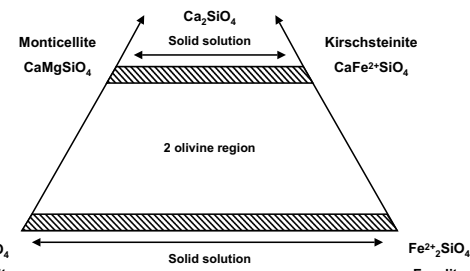


FIGURE 3. The olivine quadrilateral. See text for discussion.

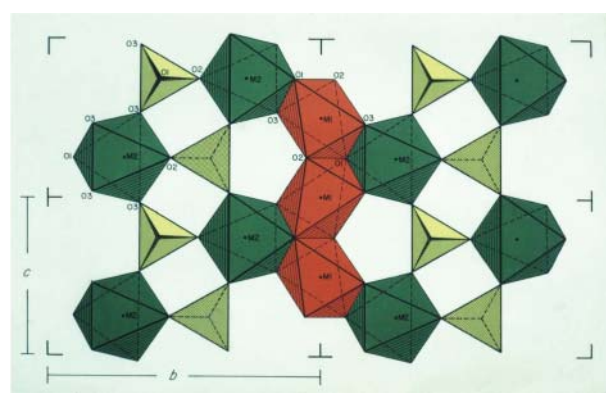
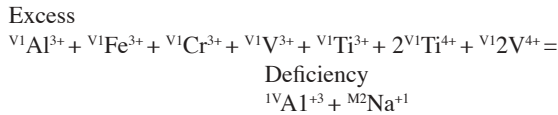


FIGURE 4. Crystal structure of olivine. See text for discussion.

the Di-Hed join, whereas pigeonite is monoclinic and plots near the En-Fs join. Orthopyroxene occurs near the En-Fs join and usually has lower Ca contents than pigeonite.

Pyroxene in the “Others” group deviates from “Quad” pyroxene according to coupled substitutions represented by the following equation (Cameron and Papike 1981):



Crystal structure types are tabulated in Table 1. The C2/c structure (Fig. 7) is the simplest of the pyroxene structures. The M1 octahedra share edges and form bands parallel to the c-axis. These are the sites of the Y cations mentioned above. The M2 sites, which are adjacent to M1, can be considered as distorted octahedra (6-coordinated) when occupied by Mn<sup>2+</sup>, Fe<sup>2+</sup>, Mg, or Li. The coordination of these sites increases to 8 when they are occupied by Na or Ca. The single tetrahedral chains have only one symmetrically distinct tetrahedron. Figure 8 shows the types of substitutions that take place in the pyroxene structure.

### Crystal chemistry of spinel

The spinel structure (Fig. 9) can be considered an almost close-packed array of oxygen atoms where one-third of the cations occupy tetrahedral sites (A sites) and two-thirds occupy octahedral sites (B sites). A spinel in this system is “normal” if a doubly charged cation such as Fe<sup>2+</sup> occupies only the tetrahedral

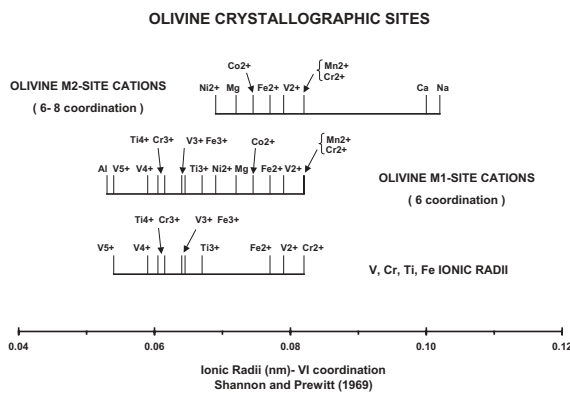


**FIGURE 5.** Possible cation substitutions in olivine based on ionic radii. See text for discussion.

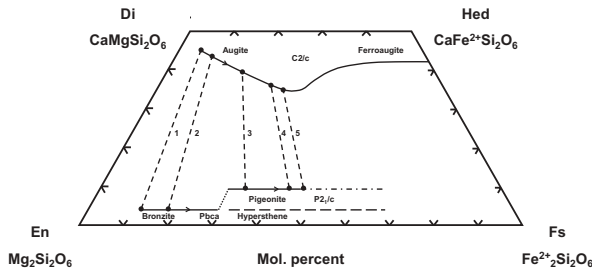


**FIGURE 6.** The pyroxene quadrilateral. See text for discussion.

sites but is “inverse” if it occupies the tetrahedral sites and half of the octahedral sites (note Table 2 for the listing of selected spinel end-members). Here we use spinel as a group name and chromite and ulvöspinel as members of the spinel group. Good reviews of spinel crystal-chemistry are provided by Waychunas

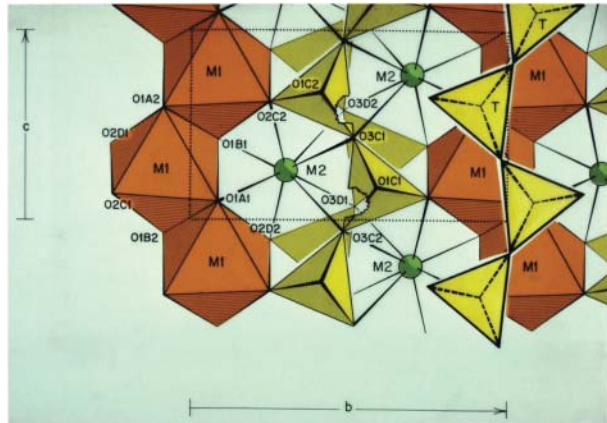


**FIGURE 7.** Crystal structure of pyroxene. See text for discussion.

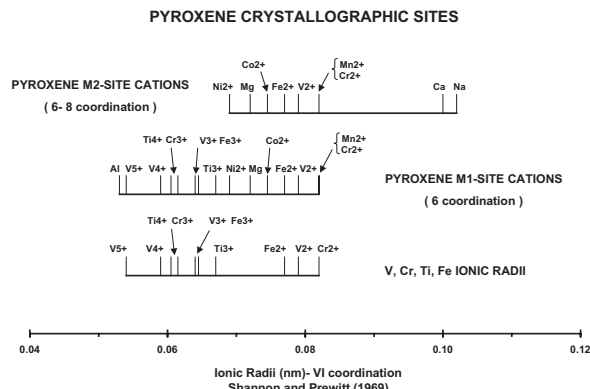


**FIGURE 8.** Possible cation substitutions in pyroxene based on ionic radii. See text for discussion.

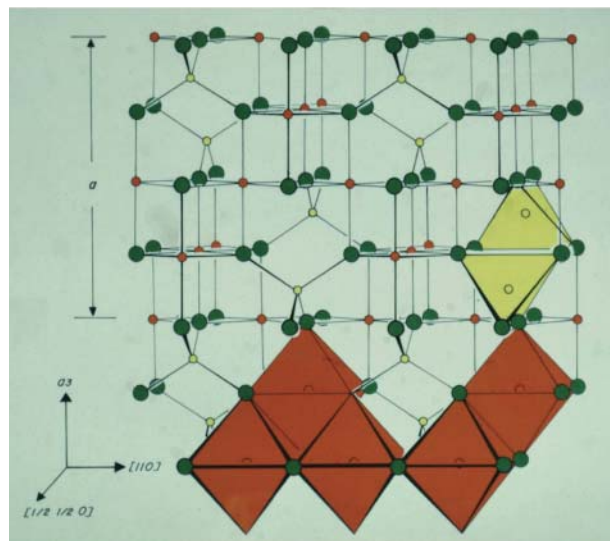


**FIGURE 9.** Crystal structure of spinel. See text for discussion.

**TABLE 1.** Major chemical subdivisions of pyroxenes (after Cameron and Papike 1980).

|                               |   |  |
|-------------------------------|---|--|
| 1. Magnesium-Iron Pyroxenes   |   |  |
| Enstatite                     | Mg <sub>2</sub> Si <sub>2</sub> O <sub>6</sub>  | Pbc <sub>a</sub> P2 <sub>1</sub> /c, Pbcn <sup>†</sup> |
| Ferrosillite                  | Fe <sup>2+</sup> Si <sub>2</sub> O <sub>6</sub>   | Pbc <sub>a</sub> P2 <sub>1</sub> /c                    |
| Orthopyroxene                 | (Mg,Fe <sup>2+</sup> ) <sub>2</sub> Si <sub>2</sub> O <sub>6</sub>  | Pbca   |
| Pigeonite                     | (Mg,Fe <sup>2+</sup> ,Ca) <sub>2</sub> Si <sub>2</sub> O <sub>6</sub>   | P2 <sub>1</sub> /c, C2/c                               |
| 2. Calcium Pyroxenes          |   |  |
| Augite                        | (Ca, R <sup>2+,*</sup> )(R <sup>2+</sup> , R <sup>3+</sup> , Ti <sup>4+</sup> )(Si, Al) <sub>2</sub> O <sub>6</sub> | C2/c   |
| Diopside                      | CaMgSi <sub>2</sub> O <sub>6</sub>  | C2/c   |
| Hedenbergite                  | CaFe <sup>2+</sup> Si <sub>2</sub> O <sub>6</sub>   | C2/c   |
| Johannsenite                  | CaMnSi <sub>2</sub> O <sub>6</sub>  | C2/c   |
| 3. Calcium – Sodium Pyroxenes |   |  |
| Omphacite                     | (Ca, Na)(R <sup>2+</sup> , Al)Si <sub>2</sub> O <sub>6</sub>  | C2/c, P2/n   |
| Aegirine - Augite             | (Ca, Na)(R <sup>2+</sup> , Fe <sup>3+</sup> )Si <sub>2</sub> O <sub>6</sub>   | C2/c   |
| 4. Sodium Pyroxenes           |   |  |
| Jadeite                       | NaAlSi <sub>2</sub> O <sub>6</sub>  | C2/c   |
| Acmite                        | NaFe <sup>3+</sup> Si <sub>2</sub> O <sub>6</sub>   | C2/c   |
| Ureyite                       | NaCr <sup>3+</sup> Si <sub>2</sub> O <sub>6</sub>   | C2/c   |
| 5. Lithium Pyroxenes          |   |  |
| Spodumene                     | LiAlSi <sub>2</sub> O <sub>6</sub>  | C2 (~C2/c)   |

\* R<sup>2+</sup> = Mn<sup>2+</sup>, Fe<sup>2+</sup>; Mg; R<sup>3+</sup> = Fe<sup>3+</sup>, Cr<sup>3+</sup>, Al.

† Multiple entries indicate polymorphs having identical composition.

**TABLE 2.** Selected spinel end-members (natural, synthesized, and predicted)

| Name                                    | Formula  |
|---|--|
| Spinel                                  | IVMg <sup>V</sup> Al <sub>2</sub> O <sub>4</sub>   |
| Hercynite                               | IVFe <sup>2+</sup> VAl <sub>2</sub> O <sub>4</sub>   |
| Chromite                                | IVFe <sup>2+</sup> VCr <sub>2</sub> O <sub>4</sub>   |
| Magnesiochromite                        | IVMg <sup>V</sup> Cr <sub>2</sub> O <sub>4</sub>   |
| Ulvöspinel                              | IVFe <sup>2+</sup> V(Fe <sup>2+</sup> Ti)O <sub>4</sub> (Inverse)  |
| Magnetite                               | IVFe <sup>3+</sup> V(Fe <sup>2+</sup> Fe <sup>3+</sup> )O <sub>4</sub> (Inverse)   |
| Coulsonite                              | IVFe <sup>2+</sup> V <sub>2</sub> O <sub>4</sub>   |
| Magnesiocoulsonite                      | IVMg <sup>V</sup> V <sub>2</sub> O <sub>4</sub>  |
| Synthetic compound (Rogers et al. 1963) | IVFe <sup>2+</sup> V(Fe <sup>2+</sup> V <sup>4+</sup> )O <sub>4</sub>  |
| Predicted                               | IV(Mg, Fe <sup>2+</sup> )V <sub>2</sub> O <sub>4</sub>   |
| Predicted (Ulmer and White 1966)        | IV(Cr <sup>3+</sup> )V <sub>2</sub> O <sub>4</sub>   |
| Space Group                             | Fd3m isometric Z = 8   |
| Normal                                  | 8R <sup>2+</sup> in A-site Tetrahedral<br>16R <sup>3+</sup> in B-site Octahedral   |
| Inverse                                 | 8R <sup>3+</sup> (or 8R <sup>2+</sup> ) in A Tet., 8R <sup>2+</sup> + 8R <sup>3+</sup><br>(or 8R <sup>4+</sup> ) in B Oct. |

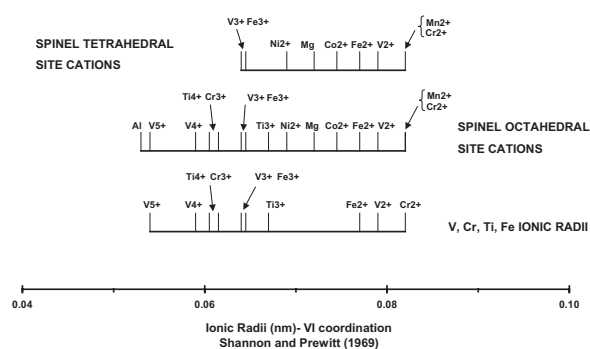
\* R<sup>2+</sup> = Mg<sup>2+</sup>, Fe<sup>2+</sup>, Cr<sup>2+</sup>; R<sup>3+</sup> = Fe<sup>3+</sup>, Cr<sup>3+</sup>, Al<sup>3+</sup>, V<sup>3+</sup>, Ti<sup>3+</sup>; R<sup>4+</sup> = Ti<sup>4+</sup>, V<sup>4+</sup>.

(1991), and for the magnetite-ulvöspinel solid solution series by Wechsler et al. (1984).

The location of cations in the structure is determined in large part by crystal-field stabilization energy, ionic radii, and valence. Octahedral site preference energies (reviewed by Haggerty 1972) probably decrease in the order Cr<sup>3+</sup> > Al<sup>3+</sup> ≥ Ti<sup>4+</sup> > Fe<sup>2+</sup>. Thus, in general, trivalent and tetravalent cations are restricted to the octahedrally coordinated B sites, whereas the divalent cations occupy either the A or B sites.

Figure 10 shows the possible cation substitutions that can take place in the octahedral and tetrahedral crystallographic sites. Figure 11 shows what takes place in a solid solution series between magnesiochromite and ulvöspinel. The structural transformation from “normal” to “inverse” in this solid-solution suite must accommodate the charge-balance requirements of the oxygen ligands. Key oxygen ligands are bound to three octahedra and one tetrahedron. Therefore the oxygen (-2 charge) must receive +2 charge from three octahedral cations and one tetrahedral cation. This relationship is illustrated in Figure 12.

## SPINEL CRYSTALLOGRAPHIC SITES

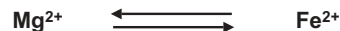
**FIGURE 10.** Possible cation substitutions in spinel based on ionic radii. See text for discussion.

## Chromite – Ulvöspinel solid solution

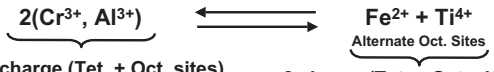


## Magnesiochromite

## Tetrahedral Site



## Octahedral Site



+ 8 charge (Tet. + Oct. sites)      + 8 charge (Tet. + Oct. sites)

Cubic: Space group Fd3m, Z=8, Unit cell a≈8.08-8.53Å, 8 Tetrahedral sites (A sites), 16 Octahedral sites (B sites)

**FIGURE 11.** Crystal-chemical aspects of solid solution between chromite and ulvöspinel. Diagram after Papike et al. (2004).

## EFFECTS OF VARIABLE OXYGEN FUGACITY ON CATION SUBSTITUTIONS

## Olivine

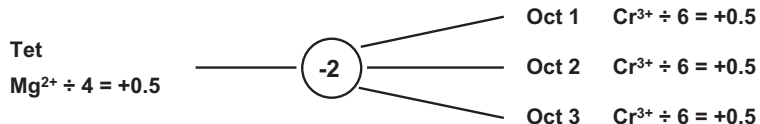
**Chromium.** The sample suites used in our comparative planetary mineralogy study of olivine are listed in Table 3. Most Cr in the Earth is Cr<sup>3+</sup> but not all, and there is a significant amount of Cr<sup>2+</sup> in lunar basalts. Hanson and Jones (1998) (Fig. 13) showed that at the IW buffer, much of the Cr in mare basalts is 2+. Clearly there is sufficient Cr<sup>3+</sup> in the mare basalts to permit early crystallization of chromite. Sutton et al. (1993) used XANES techniques to show that Cr is predominately Cr<sup>2+</sup> in lunar olivine (sample 15555) and Cr<sup>3+</sup> in pyroxene. Karner et al. (2003) showed that the high activity of Cr in lunar melts is reflected by high Cr in lunar olivine relative to olivine from the Earth or Mars (Fig. 14). This finding reflects not only the high activity of Cr in the melt, but the significant substitution of Cr<sup>2+</sup> into the olivine structure (Sutton et al. 1993). The Cr<sup>2+</sup> ion will fit into either the M2 or M1 site of olivine (Figs. 4 and 5), and substitution for Mg<sup>2+</sup> or Fe<sup>2+</sup> creates no charge-balance problems.

**TABLE 3.** Basalt suites chosen for olivine analysis, along with corresponding setting, locality, thin section number, and rock type (after Karner et al. 2003)

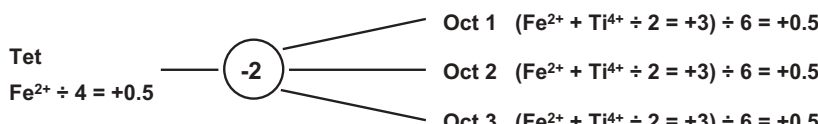
| Sample suite               | Geologic setting  | Locality  | Thin section-rock type  | References  |
|----------------------------|---|---|---|---|
| Archean                    | Archean greenstone belts                                  | Munro and Cook Townships, Ontario, Canada                                     | ARCH-4 Olivine spinifex   | Naldrett and Smith 1981                           |
| Ocean floor basalts        | Mid-ocean ridge divergent plate volcanism                 | Mid-Atlantic Ridge, Galapagos Ridge, East Pacific Rise                        | OF-1, OF-3, OF-8, Primitive basalts<br>OF-9 High-Ti basalt<br>OF-16 Evolved basalt  | Rhodes and Bence 1981                             |
| Continental rift basalts   | Extensional tectonics within continental plates           | Taos Plateau, New Mexico, USA   | TP-1 Olivine tholeiite, TP-17, TP-21 Olivine andesites  | Dungan et al. 1981                                |
| Island Arc basalts         | Volcanism onto ocean floor at convergent plate boundaries | New Britain, Papua-New Guinea   | IA-7 Porphyritic basalt<br>IA-11 Vesicular basalt   | Taylor et al. 1981                                |
| Oceanic Intraplate basalts | Oceanic-island hotspot volcanism                          | Hawaiian islands, USA   | HAW-1, HAW-22 Tholeiites, HAW-11 Alkali basalt, HAW-17 Ankaramite,  | Bence 1981  |
| Continental flood basalts  | Flood lavas produced at continental rifts                 | Keweenawan, Lake Superior Basin, N. America Columbia Plateau, Washington, USA | KEW-5 Olivine tholeiite<br>CP-4 Olivine basalt<br>CP-8 Porphyritic basalt   | Green and Haskin 1981<br>Haggerty and Irving 1981 |
| Lunar Basalts              | Lunar mare basaltic volcanism                             | Apollo (AP) 11, 12, 15 & 17 landing sites                                     | 10020, 10062 AP11 Low-K basalts;<br>12009, 12020, 12075 AP12<br>Olivine basalts; 12020, 12063 AP12<br>Ilmenite basalts; 15016, 15545 AP15<br>Olivine basalts; 70215, 74275 AP17<br>Very High-Ti basalts | Papike et al. 1976                                |
| Martian Basalts            | Martian basaltic volcanism                                | Meteorites-Dar al Gani 476, LEW 88516, and ALH 77005                          | Dar al Gani 476 Basaltic shergottite<br>LEW 88516, ALH 77005<br>Lherzolitic shergottites  | McSween and Treiman. 1998                         |

### Oxygen charge balance requirements in spinel (Oxygen ligands bonded to three octahedra and one tetrahedron require 2+ charges)

#### A. Magnesiochromite $\text{IV}^{\text{Mg}}\text{VI}^{\text{Cr}^{3+}}\text{Cr}_2\text{O}_4$ (Normal)



#### B. Ulvöspinel $\text{IV}^{\text{Fe}^{2+}}\text{VI}^{\text{(Fe}^{2+} + \text{Ti}^{4+})}\text{O}_4$ (Inverse)



#### C. Magnetite $\text{IV}^{\text{Fe}^{3+}}\text{VI}^{\text{(Fe}^{3+} + \text{Fe}^{2+})}\text{O}_4$ (Inverse)



**FIGURE 12.** Crystal-chemical aspects of charge-balance requirements of oxygen ligands in the spinel structure. See text for discussion.

However,  $\text{Cr}^{3+}$  requires either a  $\text{M}^2\text{Na}^{+1-\text{M}1}\text{Cr}^{3+}$  couple or  $\square\text{-}2\text{Cr}^{3+}$  couple. Despite this difference in substitutional mechanism of  $\text{Cr}^{2+}$  and  $\text{Cr}^{3+}$  into the olivine structure, the  $D$ -values for both in olivine are remarkably similar (Hanson and Jones 1998). In fact,  $D_{\text{Cr}}$  (olivine/melt) remains fairly constant at  $\sim 0.6$  over a large range of  $f_{\text{O}_2}$  (Fig. 15) (Mikouchi et al. 1994; Gaetani and Grove

1996). The similarity in  $D_{\text{Cr}}^{3+}$  and  $D_{\text{Cr}}^{2+}$  in olivine is probably because, although  $\text{Cr}^{2+}$  substitution for  $\text{Mg}^{2+}$  or  $\text{Fe}^{2+}$  causes no charge-balance problems, the  $\text{Cr}^{2+}$  cation is almost too big for the olivine M1 site (similar to  $\text{Mn}^{2+}$ , see Fig. 8). By contrast, the  $\text{Cr}^{3+}$  ion fits nicely into the olivine M1 site (Fig. 8). Although  $\text{Cr}^{2+}$  and  $\text{Cr}^{3+}$  are both incompatible in olivine, Figure 14 shows that Cr decreases significantly in olivine with fractionation. We use Mn here as an igneous fractionation indicator, as it behaves incompletely in olivine (Papike et al. 1999). The behavior of Cr (i.e., decreasing with crystallization), is similar to that of Ni, which is a highly compatible element in olivine. We believe this trend is largely the result of early chromite crystallization, which depletes the evolving melt in Cr. The likely reason for the high Cr abundance in lunar olivine stems from the fact that lunar melts have high Cr contents and

significant  $\text{Cr}^{2+}$ . The activity of  $\text{Cr}^{2+}$  in the melts is high (Hanson and Jones 1998), and will partition into early crystallizing olivine. This scenario is supported by the XANES work of Sutton et al. (1993), which showed that Cr in lunar olivine was predominantly divalent.

**Titanium.** The variation of Ti in olivine from lunar (Low-

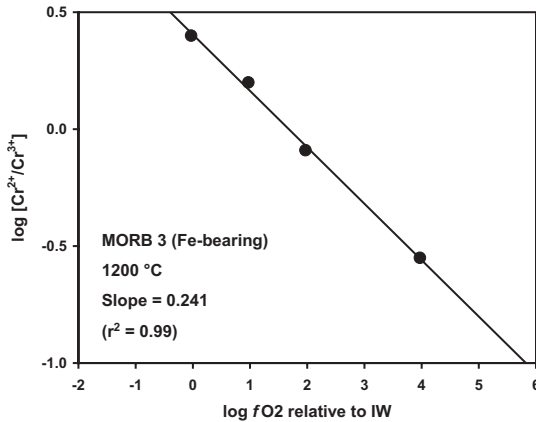


FIGURE 13. Log  $\text{Cr}^{2+}/\text{Cr}^{3+}$  vs.  $\log f_{\text{O}_2}$  relative to IW. Diagram after Hanson and Jones (1998).

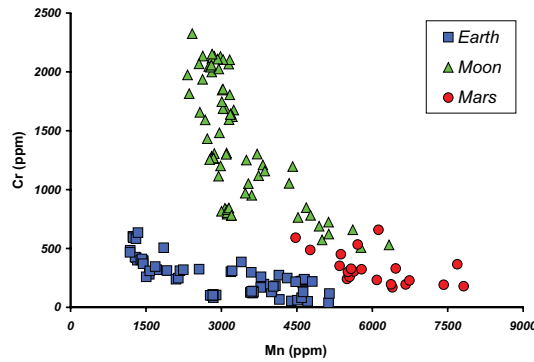


FIGURE 14. Variation of Cr (ppm) and Mn (ppm) in olivine from planetary basalts. Manganese behaves incomparably in olivine, and thus can be used as an indicator of igneous fractionation. After Karner et al. (2003).

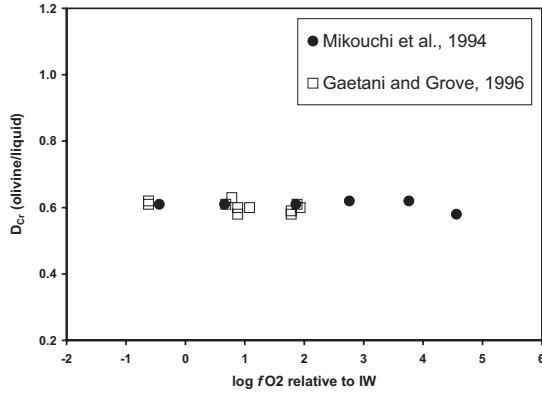


FIGURE 15.  $D_{\text{Cr}}$  (olivine/liquid) vs.  $\log f_{\text{O}_2}$  relative to IW. After Hanson and Jones (1998).

Ti basalts only), martian, and terrestrial basalts is illustrated in Figure 16. In these low-Ti melts, olivine is slightly enriched in Ti content with crystallization (i.e., increasing Mn) because Ti is incompatible in early crystallizing phases, including chromite. Ulvöspinel, however, will take up significant  $\text{Ti}^{4+}$  in the late stages of crystallization. The high concentration of Ti in most

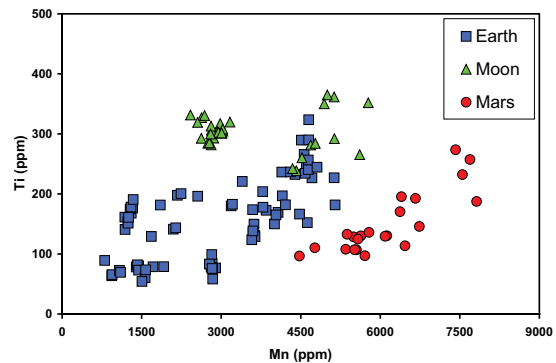


FIGURE 16. Variation of Ti (ppm) and Mn (ppm) in olivine from planetary basalts. Manganese is used as an indicator of increasing crystallization, as it behaves incomparably in olivine. After Karner et al. (2003).

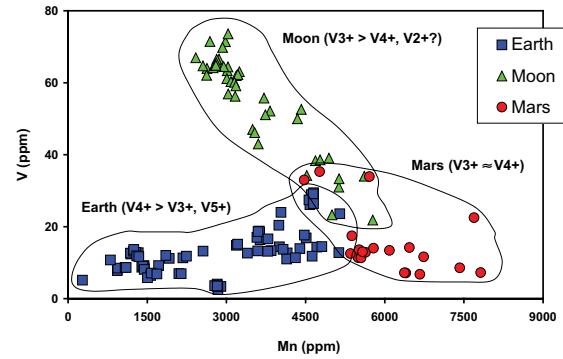


FIGURE 17. Variation of V (ppm) and Mn (ppm) in olivine from planetary basalts. Manganese is used as an indicator of increasing crystallization, as it behaves incomparably in olivine. After Karner et al. (2003).

lunar olivine reflects the compositionally diverse source regions on the Moon (e.g., higher  $\text{TiO}_2$ ) relative to the Earth and Mars, and might reflect a small  $\text{Ti}^{3+}$  component.

**Vanadium.** Our V in olivine data for Earth, Moon, and Mars is illustrated in Figure 17. It shows clearly that V in olivine from the Moon is significantly enriched relative to Earth or Mars. This variation is almost certainly a result of the low  $f_{\text{O}_2}$  realized by lunar basalt magmatism (~IW-1). The low  $f_{\text{O}_2}$  of the Moon results in high  $\text{V}^{3+}/\text{V}^{4+}$  for lunar melts but may also result in some  $\text{V}^{2+}$ .  $\text{V}^{2+}$  would fit nicely into either the M1 or M2 site in olivine (Fig. 8) and also creates no charge-balance problems. However,  $\text{V}^{2+}$  is probably low in abundance, if it exists at all in lunar melts at IW-1. Therefore, the high concentration of V in lunar olivine relative to olivine from Mars or Earth must be the result of  $D_V$  (olivine/melt) for  $\text{V}^{3+}$  being significantly larger than for  $D_{\text{V}^{4+}}$  (Canil and Fedortchouk 2001), because the range of V concentrations in the basalts from the three planets is not that different. The  $\text{V}^{3+}-\text{V}^{4+}$  partitioning difference is probably due to charge-balance rather than ionic radii (Fig. 5), because both fit nicely into the olivine octahedral sites. The substitutional couple  $\square-\text{V}^{3+}$  is probably easier for the olivine structure to accommodate (more compatible) than  $\square-\text{V}^{4+}$ . In other words, one vacancy accommodates  $2\text{V}^{3+}$  cations whereas one vacancy

accommodates only one  $V^{4+}$  cation. For example, note the two following exchange reactions:



### Pyroxene

**General.** For some of the following plots, the data for terrestrial basalt pyroxene are presented as averages for each of seven sample suites: Archean, Columbia Plateau, Ocean Floor, Hawaiian, Island Arc, Keweenawan, and Rio Grande (Papike 1998). Therefore, some of the data displays for terrestrial pyroxene only contain seven points, but these points actually represent 1263 analyses (Papike 1981). The details concerning these basalt suites are reported in BVSP (1981) and a specific discussion of the silicate mineralogy is reported by Papike (1981). The pyroxene data for lunar mare basalts are tabulated in the appendix to Papike et al. (1998). Data for the pyroxene in martian rocks are from McSween and Trieman (1998). Statistical analysis of the data for pyroxene chemical analysis from BVSP (1981) is reported by Papike and White (1979), Papike (1980), and Papike (1981). For a complete coverage of these studies, refer to those papers. However, Table 4 is a brief summary of results specifically on the relative importance of "Others" components (discussed above) in pyroxene from different planetary basalt suites. Several things are important to note: (1) The importance of  $Fe^{3+}$  in terrestrial basaltic pyroxene.  $M^1Fe^{3+}-IVAl^{3+}$  or  $M^2Na^{1+}-M^1Fe^{3+}$  are either the first or second most important substitutional couple in six of the seven terrestrial suites studied; (2)  $M^1Ti^{4+}-2IVAl^{3+}$  is a very important charge couple in eight of the nine suites studied, and; (3) The importance of  $M^2Na-M^1Al^{3+}$

**TABLE 4.** Summary of relative importance of pyroxenes "others" cation couples (after Papike and White 1979)

| Group            | First most important | Second most important |
|------------------|----------------------|-----------------------|
| Archean          | $M^1Ti - 2^{VI}Al$   | $M^1Al - IVAl$        |
| Columbia Plateau | $M^1Fe^{3+} - IVAl$  | $M^1Ti - 2^{VI}Al$    |
| Deep Sea         | $M^1Ti - 2^{VI}Al$   | $M^1Fe^{3+} - IVAl$   |
| Shergotty (Mars) | $M^1Ti - 2^{VI}Al$   | $M^2Na - M^1Al$       |
| Hawaiian         | $M^1Ti - 2^{VI}Al$   | $M^2Na - M^1Fe^{3+}$  |
| Island Arc       | $M^1Al - IVAl$       | $M^1Fe^{3+} - IVAl$   |
| Keweenawan       | $M^1Fe^{3+} - IVAl$  | $M^1Ti - 2^{VI}Al$    |
| Lunar Mare       | $M^1Ti - 2^{VI}Al$   | $M^1Al - IVAl$        |
| Rio Grande       | $M^1Fe^{3+} - IVAl$  | $M^1Ti - 2^{VI}Al$    |

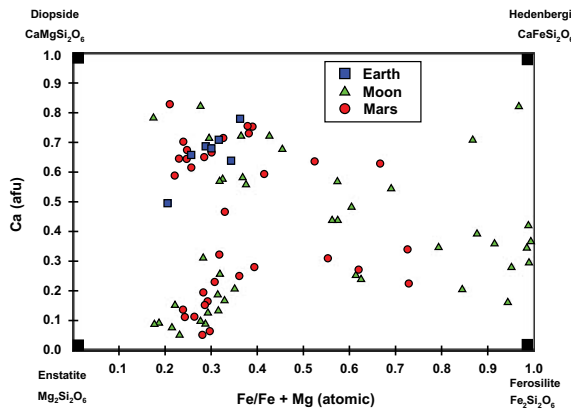
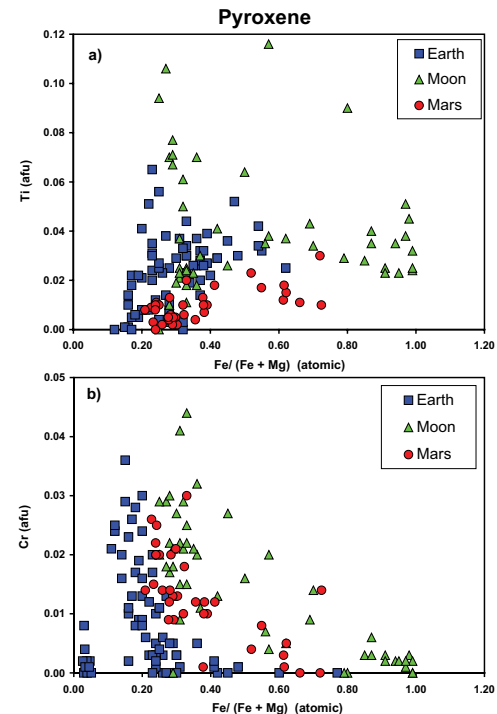


**FIGURE 18.** Ca (afu) vs. Fe/(Fe + Mg) (atomic) for pyroxene in planetary basalts. After Papike (1998).

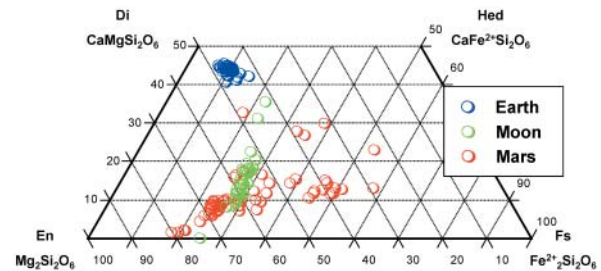
in Shergotty (martian) pyroxene reflecting the high abundance of Na in Mars (Papike 1998). This jadeite component on Earth usually indicates high pressure conditions, however, the low concentrations in martian pyroxene do not imply this.

Figure 18 is a data display very similar to the familiar pyroxene quadrilateral plot but instead plots atoms per formula unit (afu) of Ca versus  $Fe^{2+}/(Fe^{2+} + Mg)$  (atomic) in pyroxene. A significant noteworthy feature of this diagram is the almost total overlap of pyroxene compositions for lunar and martian basalts. For detailed major- and minor-element data for the terrestrial pyroxene suites, consult Papike (1981).

**Chromium and Titanium.** Figures 19a and 19b display the Ti (afu) vs.  $Fe/(Fe + Mg)$  (atomic) and Cr (afu) vs.  $Fe/(Fe + Mg)$  (atomic) data for pyroxene. Here we plot 70 terrestrial pyroxene analyses from BVSP (1981), 10 from each of the seven terrestrial suites. Figure 19a shows that generally pyroxene from lunar basalts contains higher Ti than either martian or terrestrial pyroxene. This difference likely reflects the higher concentration of Ti in



**FIGURE 19.** Ti (afu) vs.  $Fe/(Fe + Mg)$  (atomic) and Cr (afu) vs.  $Fe/(Fe + Mg)$  (atomic) for pyroxene in planetary basalts. After Papike (1998).



**FIGURE 20.** Compositions for pyroxene used in the V in pyroxene discussion in this paper. See text for discussion.

mare basalts (even though we have not plotted lunar pyroxene from the High-Ti basalts) as compared to martian and terrestrial basalts. Another factor could be that  $\text{Fe}^{3+}$  competes with  $\text{Ti}^{4+}$  for the M1 site in pyroxene, thus martian and terrestrial pyroxene have lower Ti than lunar pyroxene. Figure 19b displays pyroxene Cr data and shows that although lunar olivine (discussed above) has quite elevated Cr contents relative to olivine from Mars or Earth, this is not true for lunar pyroxene (note also Papike 1981). This difference reflects the fact that Cr in lunar basaltic melts is largely  $\text{Cr}^{2+}$  and goes into olivine, whereas the  $\text{Cr}^{3+}$  activity of lunar basalts is more similar to the  $\text{Cr}^{3+}$  activity of martian and terrestrial basaltic melts.

**Vanadium.** In order to be able to discuss V in pyroxene from planetary basalts, we collected new data on a small set of representative samples from Earth, Moon, and Mars. The samples we used for this study are a terrestrial Hawaiian basalt-HAW-17 (note Table 3); two basaltic meteorites from Mars- Shergotty and Dar al Gani 476 (note Meyer 2003); and a lunar olivine basalt-12075 (note Papike et al. 1998). The quadrilateral systematics for these four samples are shown in Figure 20. These data were used to locate our SIMS points for V analysis. Figure 21 shows the variation of V in lunar, martian, and terrestrial pyroxene as a function of Ca content and  $\text{Fe}/(\text{Fe} + \text{Mg})$  (atomic). Figure 22 shows these same data but now normalized to the bulk V content of the rock. Note these ratios are not D-values because some of these basalts are cumulates and the  $V_{\text{pyroxene}}/V_{\text{rock}}$  does not represent the equilibrium distribution of V between pyroxene and V of the coexisting melt. Nevertheless, these plots give some

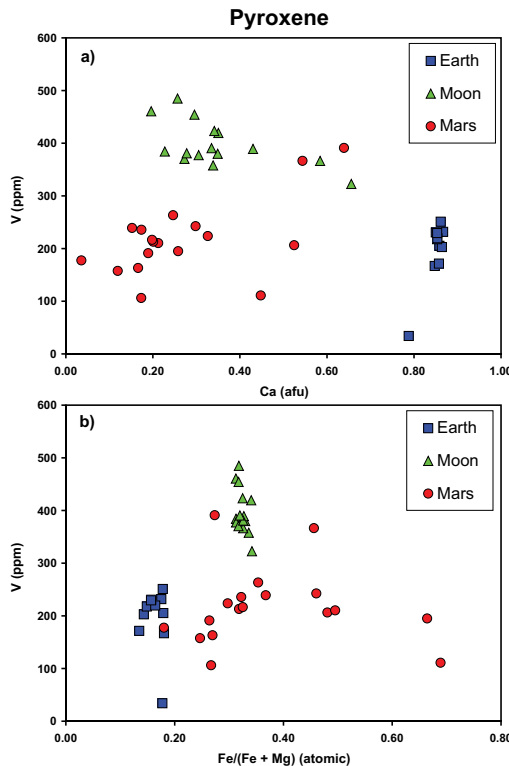


FIGURE 21. (a) V (ppm) and Ca (afu) variation in pyroxene from planetary basalts. (b) V (ppm) and  $\text{Fe}/(\text{Fe} + \text{Mg})$  (atomic) variation in pyroxene from planetary basalts. See text for discussion.

significant insights concerning V partitioning between pyroxene and basaltic melt. First, the partitioning of V appears to be little affected by either Ca content or  $\text{Fe}/(\text{Fe} + \text{Mg})$  (atomic) of the pyroxene. However, Toplis and Corgne (2002) state that  $D_{V^{3+}}$  (Cpx/Liq.) increases as the pyroxene becomes more Fe-rich. The most important controlling factor from our studies is the low  $f_{\text{O}_2}$  for lunar basalts (IW-1) relative to the higher  $f_{\text{O}_2}$  conditions for the Earth and Mars. The low  $f_{\text{O}_2}$  on the Moon results in very high  $V^{3+}/V^{4+}$  for lunar melts, and subsequently high concentrations of V in lunar pyroxene. These systematics also demonstrate that the charge-balance couple  $\text{M}^{\text{IV}}\text{V}^{3+}-\text{IVAl}$  is much more compatible in the pyroxene crystal structure than  $\text{M}^{\text{IV}}\text{V}^{4+}-\text{IVAl}$ .

**Titanium vs. aluminum systematics.** Figure 23 is a plot of Ti (afu) vs. Al (afu). The Ti/Al line of 1/2 reflects the important  $\text{M}^{\text{IV}}\text{Ti}^{4+}-\text{IVAl}^{3+}$  couple discussed above. Points that plot below this line reflect additional components like  $\text{M}^{\text{IV}}\text{Al}-\text{IVAl}$ ,  $\text{Fe}^{3+}-\text{IVAl}$ , or  $\text{Na}-\text{IVAl}$ . Points that plot above the Ti/Al = 1/2 line give some indication of the presence of  $\text{Ti}^{3+}$  as the couple  $\text{M}^{\text{IV}}\text{Ti}^{3+}-\text{IVAl}^{3+}$ . Thus, this is evidence for minor  $\text{Ti}^{3+}$  concentrations in lunar pyroxene grains that crystallized at oxygen fugacities of ~IW-1 (Jones 2004). However, it does not appear that  $\text{Ti}^{3+}$  is a major component in lunar mare basalts. On the other hand,  $\text{Ti}^{3+}$  is a very important component of the Ti in pyroxene from Ca-Al-rich inclusions (CAIs); (type B) in carbonaceous chondrites that crystallized at  $f_{\text{O}_2} \sim 10^{-19}$  at 1200 °C, which is ~IW-7 (Sutton et al. 2002). In these pyroxene grains,  $\text{Ti}^{3+}$  and  $\text{Ti}^{4+}$  are approximately equal in abundance. The oxygen fugacities realized in the Moon simply do not produce much  $\text{Ti}^{3+}$ .

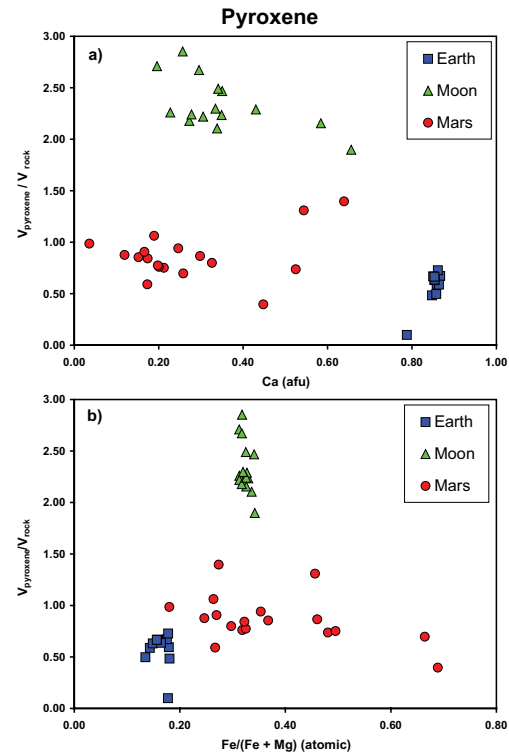
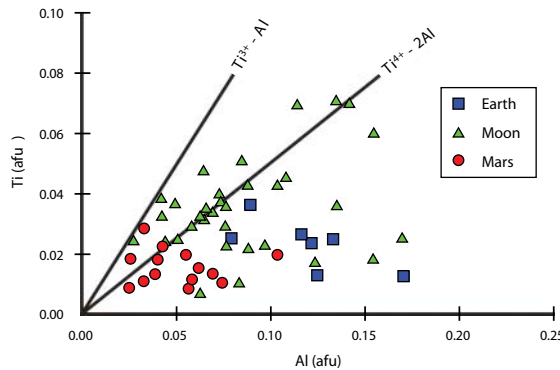


FIGURE 22. (a)  $V_{\text{pyroxene}}/V_{\text{rock}}$  vs. Ca (afu) in pyroxene from planetary basalts. (b)  $V_{\text{pyroxene}}/V_{\text{rock}}$  vs.  $\text{Fe}/(\text{Fe} + \text{Mg})$  (atomic) in pyroxene from planetary basalts. See text for discussion.

**TABLE 5.** Basalt suites chosen for chromite analysis, along with corresponding setting, locality, thin section number, and rock type

| Sample suite               | Geologic setting  | Locality                               | Thin section-rock type   | Reference   |
|----------------------------|---|--|--|---|
| Ocean floor basalts        | Mid-ocean ridge, divergent plate volcanism                | Mid-Atlantic Ridge                     | OF-3 Primitive basalt  | Rhodes and Bence 1981   |
| Island Arc basalts         | Volcanism onto ocean floor at convergent plate boundaries | New Britain, Papua-New Guinea          | IA-11 Vesicular basalt   | Taylor et al. 1981  |
| Oceanic Intraplate basalts | Oceanic-island hotspot volcanism                          | Hawaiian islands, USA                  | HAW-17 Ankaramite<br>Kilauea Iki-1 Olivine tholeiite<br>Makaopuhi-22 Olivine tholeiite           | Bence 1981<br>Shearer (Personal Comm.)<br>Wright and Okamura 1977 |
| Lunar Basalts              | Lunar mare basaltic volcanism                             | Apollo (AP) 12 & 15 landing sites      | 12020, 12075 AP12 Olivine basalts;<br>12063 AP12 Ilmenite basalt;<br>15595 AP15 Pigeonite basalt | Papike et al. 1976  |
| Martian Basalts            | Martian basaltic volcanism                                | Meteorites-Dar al Gani 476, EETA 79001 | Dar al Gani 476, EETA 79001 Basaltic shergottites  | Meyer 2003  |



**FIGURE 23.** Ti (afu) vs. Al (afu) for pyroxene from planetary basalts. After Papike (1998).

### Spinel

**General.** We now address the systematics of Cr, Ti, and V in spinel and the behavior of V valence-states in chromite in basalts from Earth, Moon, and Mars. The sample suite used for this study is reported in Table 5. Additional data for martian chromite grains are provided by Goodrich et al. (2003).

**Vanadium, chromium, and titanium.** We have been looking for a “V in chromite oxybarometer” that works with data collected by the electron microprobe and thus is readily accessible to a large segment of the planetary materials community. Several previous workers have recognized the potential of using V valence to estimate oxygen fugacity, e.g., Lindstrom (1976); Shervais (1982); Canil (1999, 2002); Pearce et al. (2000); Canil and Fedortchouk (2001); Delano (2001); Toplis and Corrigan (2002); and Connolly and Burnett (2003). One paper of particular importance to our present work on chromite is Canil (2002), because he did partitioning studies of V between several basalt and chromite compositions and showed that for high Cr/Al,  $D_V$  spinel/melt increases dramatically from ~5 at high  $f_{O_2}$  (IW+4) to ~32 at low  $f_{O_2}$  (IW-1).

Our first insights into developing a “V in chromite oxybarometer” resulted from performing electron probe traverses across spinel grains, analyzing for Cr, Al, Ti, Fe, Mg, Mn, and V from core to rim on grains that show zoning from chromite to ulvöspinel. Four typical zoning profiles are illustrated in Figures 24 and 25. Note that the zoning between chromite and ulvöspinel is usually not continuous but is instead an abrupt break between core and rim (Papike et al. 1976; Goodrich et al. 2003). Figure

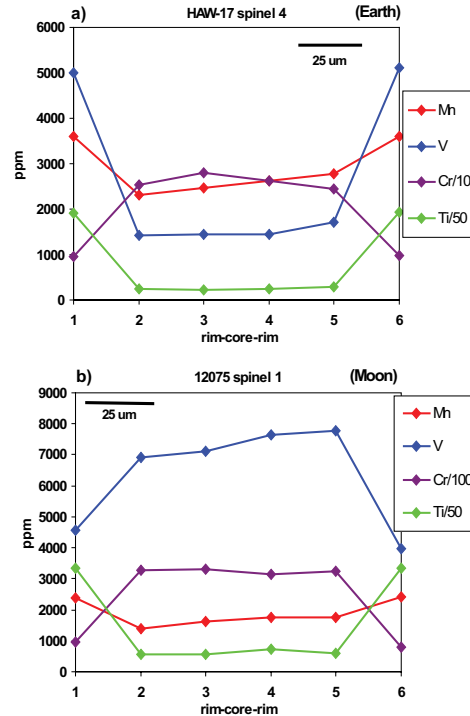


**FIGURE 24.** Typical zoning profiles for a terrestrial spinel grain from a Hawaiian (HAW-17) basalt and for a spinel from lunar basalt 12075. Traverses were done on grains that zoned from chromite cores to Fe-Ti spinel rims, with approximately 25  $\mu\text{m}$  steps. After Papike et al. 2004.

24a is for a terrestrial chromite from a Hawaiian basalt and Figure 24b is for a chromite from a lunar basalt. The zoning profiles of all spinel grains studied show the normal trends of core to rim decreases of Cr, Al, and Mg, and increases of Fe, Ti and Mn. However, much to our surprise and delight, the V behavior was very different for the Moon and Earth. In terrestrial basalts  $V^{4+} > V^{3+}$ , in lunar basalts  $V^{3+} > V^{4+}$ , and in martian basalts  $V^{3+}$  and  $V^{4+}$  are both significant (Karner et al. 2004a). The trends (core to rim) for the Moon show a strong positive correlation for V and Cr and a negative correlation for V and Ti. In terrestrial spinel, the trends are just the opposite, with strong negative correlation for V and Cr and a strong positive correlation for V and Ti. Spinel in martian basalts (Fig. 25) shows trends somewhere in between, with DaG 476 (Fig. 25a) showing lunar-type trends and EETA

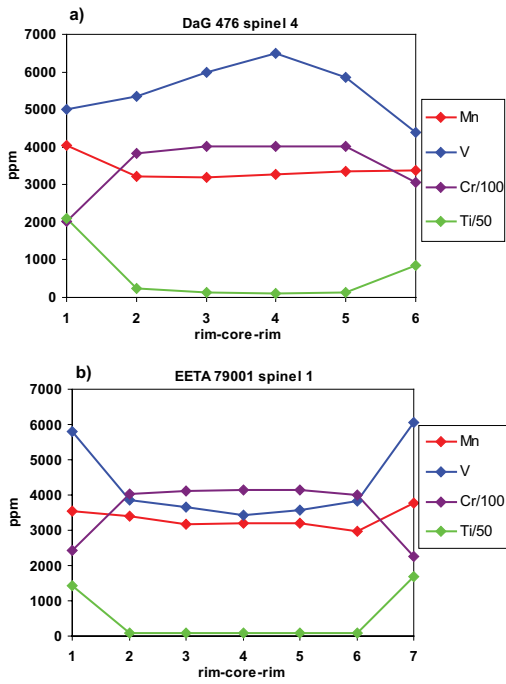


**FIGURE 25.** Typical zoning profiles for two spinel grains from martian basalts. Traverses were done on grains that zoned from chromite cores to Fe-Ti spinel rims, with approximately 25  $\mu\text{m}$  steps.

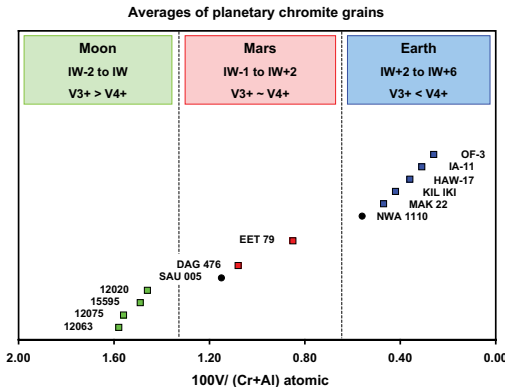


**FIGURE 26.** Average  $100V/(Cr + Al)$  (atomic) ratios for chromite grains from planetary basalts. Also shown are the  $f_{O_2}$  ranges estimated for materials from Earth, Moon and Mars, along with the relative proportions of  $V^{3+}$  and  $V^{4+}$  in these bodies. The squares are data from this study, while the dots are data from Goodrich et al. (2003). After Papike et al. 2004.

79001 (lithology A) (Fig. 25b) showing terrestrial-type trends. According to Wadhwa (2001) and Herd et al. (2002), EETA 79001 (lithology A) crystallized at a higher  $f_{O_2}$  than DaG 476.

A convenient way to display the data for chromite cores is a plot showing the relative  $V/(Cr + Al)$  ratios (Fig. 26). Because  $D_V$  increases with decreasing  $f_{O_2}$ , the trend of these ratios nicely differentiate the  $f_{O_2}$  ranges for Earth, Moon, and Mars. Thus, it appears these simple measurements, using only an electron microprobe on single chromite grains, can yield significant qualitative data about planetary parentage and relative  $f_{O_2}$ . This technique would be particularly useful for isolated chromite grains from

a planetary regolith, which will probably be the main type of sample returned from future planetary missions.

Of course, much more quantitative estimates of  $f_{O_2}$  can be made when we have a basalt that represents a melt (not a cumulate) containing chromite that is in equilibrium with the melt. Such rocks are not easy to find in planetary environments where our sample suite is small. For example, both martian rocks used in this study are cumulates, not melts, which is why we use the term mineral/rock rather than mineral/melt. Nevertheless, we have tried to move this new chromite technique one step further. The attempt was enabled by the work of Canil (2002) (Fig. 27) who reported  $D_V$  chromite/liquid over a range of  $f_{O_2}$  values from IW+4 to IW-1. In Figure 28a, we used our measured V in chromite with literature values of V in the rock (usually not a melt) to calculate “ $D$ -values” and plot them vs.  $\log f_{O_2}$  as determined by Canil (2002). Figure 28b is a plot of our ratio  $100V/(Cr + Al)$  plotted in the same way. Figure 28c is derived from the V valence determination work described in Sutton et al. (2005) and Karner et al. (2004a).

Recently Righter et al. (2004) used XANES techniques to study the valence state of V in spinel at relatively high  $f_{O_2}$  between the Nickel-Nickel Oxide (NNO) and Hematite-Magnetite (HM) buffers (i.e.,  $\sim$ IW+4 to IW+10). Although this work was done at higher  $f_{O_2}$  conditions than we have been considering, the results show that spinel grains grown at varying  $f_{O_2}$  values near NNO all have similar pre-edge peak intensities, but spinel grains grown near HM have a much higher pre-edge peak intensity. Furthermore, glass has a higher pre-edge peak intensity than coexisting spinel in all cases. Application of the glass calibration (to relate pre-edge peak intensity to valence) indicates that the three lowest  $f_{O_2}$  glasses are dominated by  $V^{4+}$ , whereas the highest  $f_{O_2}$  glass (HM) contains mixed V valences of 4+ and 5+. Although measurements on spinel grains of known V valence are required to calibrate these spectra, the glass calibration provides some preliminary insight (particularly appropriate if V in spinel resides in octahedral sites). In this case, the results suggest that spinel is dominated by  $V^{3+}$ , except for the most oxidized system (HM), which is inferred to be dominated by  $V^{4+}$ .

The chemical systematics for Ti-V-(Cr + Al) in planetary chromite grains are illustrated on a ternary diagram (Fig. 29). The spinel compositions zone from chromite cores toward ulvöspinel rims, usually with a crystallization gap in between (Papike et al. 1976; Goodrich et al. 2003), but here we only include chromite compositions. The slightly higher Ti content of some lunar chromite grains could be interpreted as indicating some  $Ti^{3+}$  in the spinel structure as a  $^{IV}(Fe^{2+}, Mg)^{VI}Ti^{3+}O_4$  component. However, because lunar Low-Ti basalts (we have not included High-Ti basalts in this study) have higher Ti contents than martian or terrestrial basalts, this interpretation is not certain.

## SUMMARY STATEMENT

In this review paper we have considered the valence-state partitioning of Cr, Fe, Ti, and V over crystallographic sites in olivine, pyroxene, and spinel from planetary basalts. The sites that accommodate these cations are the M2 site (6 to 8 coordinated) and M1 site (6 coordinated) in pyroxene, the M2 site (6 to 8 coordinated) and M1 site (6 coordinated) in olivine, and the tetrahedral and octahedral sites in spinel. The samples we studied are basalts from Earth, Moon, and Mars, which have  $f_{O_2}$

conditions that range from IW-2 (Moon) to IW+6 (Earth) with Mars somewhere between at IW to IW+2. In this range of  $f_{O_2}$  the significant players are (from low to high  $f_{O_2}$ )  $Ti^{4+}$ ,  $V^{3+}$ ,  $Fe^{2+}$ ,  $Cr^{2+}$ ,  $Cr^{3+}$ ,  $V^{4+}$ , and  $Fe^{3+}$ .  $V^{2+}$  and  $Ti^{3+}$  play a minor role in

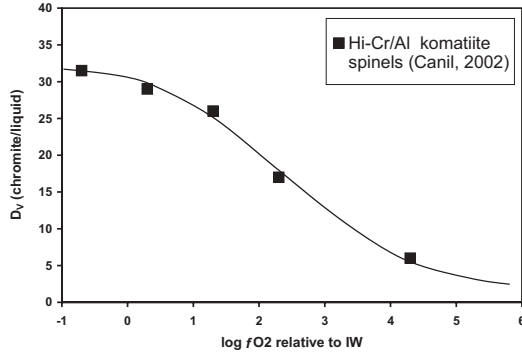


FIGURE 27.  $D_V$  (chromite/liquid) vs.  $\log f_{O_2}$  relative to IW. After Canil (2002).

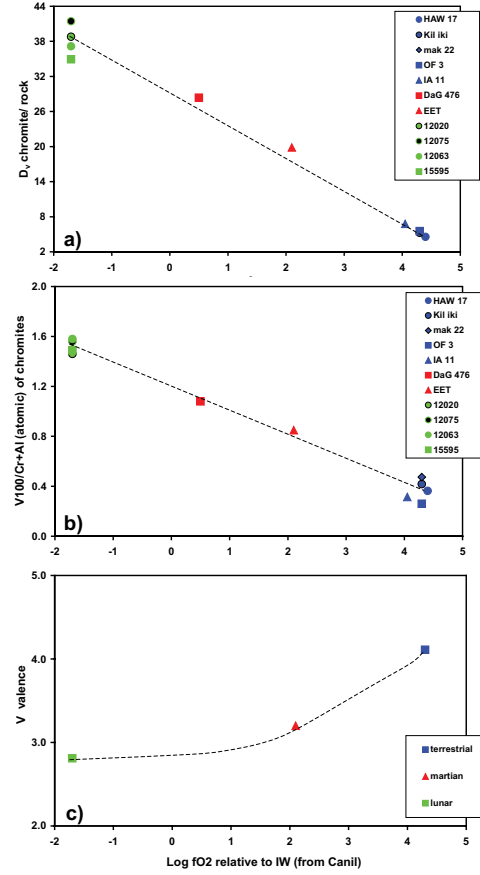


FIGURE 28. Stacked diagram showing the relationships of  $D_V$  chromite/rock,  $100V/(Cr + Al)$  (atomic) of chromite, and V valence with  $\log f_{O_2}$  relative to IW, for planetary basalts. In Figure 28a,  $D_V$  was determined by using our measured V in chromite with literature values of V in the rock;  $\log f_{O_2}$  values (X-axis) were calculated from Canil (2002). Figure 28b is a plot of our ratio  $100V/(Cr + Al)$  plotted in the same way. Figure 28c is derived from the work described in Sutton et al. (2005) and Karner et al. (2004a). All trend lines are approximate. Diagram after Papike et al. 2004.

the phases considered for the Moon, and are probably in very low concentrations.  $V^{5+}$  plays a minor role in these phases in terrestrial basalts because it is probably in lower abundance than  $V^{4+}$  and it has an ionic radii that is so small (0.054 nm, 6-coordinated, Shannon and Prewitt 1969) that it is almost at the lower limit for octahedral coordination (see Fig. 2). The role of  $Cr^{2+}$  in the Moon is significant, as Sutton et al. (1993) found that

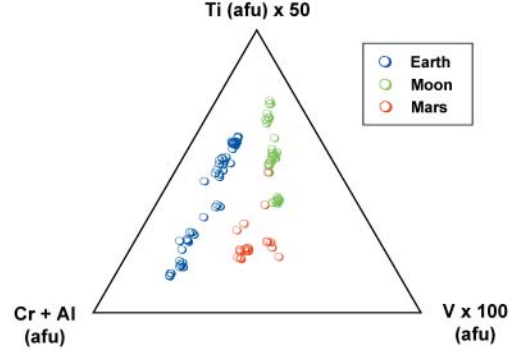


FIGURE 29. Ternary diagram for chromite showing variation of  $Ti$  (afu)  $\times 50$  vs.  $V$  (afu)  $\times 100$  vs.  $Cr + Al$  (afu). See text for discussion.

TABLE 6. How  $f_{O_2}$  conditions for the planets affect the presence and distribution of Fe, Cr, V, and Ti valence states.

| $f_{O_2}$ range for planetary basalts                           | Mars-IW-2 to IW                                 | Mars-IW to IW+2                            | Earth-IW+2 to IW+6 |
|---|---|--|--------------------|
| <b>Multivalent elements in basaltic melts</b>                   |   |  |                    |
| No $Fe^{3+}$  | $Fe^{3+}$ moderate                              | $Fe^{3+}$ high                             |                    |
| $Cr^{3+}$ moderate, $Cr^{2+}$ high                              | $Cr^{3+}$ high, $Cr^{2+}$ low                   | mostly $Cr^{3+}$ , $Cr^{2+}$ very low      |                    |
| $V^{3+} > V^{4+}$ , low $V^{2+}$                                | $V^{4+} \approx V^{3+}$                         | $V^{4+} > V^{3+}, V^{5+}$                  |                    |
| $Ti^{4+}, Ti^{3+}$ low  | all $Ti^{4+}$                                   | all $Ti^{4+}$                              |                    |
| <b>Olivine components and charge balance couples = "others"</b> |   |  |                    |
| none  | $M_2\Box M_1^2Fe^{3+}$                          | $M_2\Box M_1^2Fe^{3+}$                     |                    |
| low   | $M_2\Box M_1^2Cr^{3+}$                          | $M_2\Box M_1^2Cr^{3+}$                     |                    |
| none  | $M_2Na - M_1Cr^{3+}$                            | $M_2Na - M_1Cr^{3+}$                       |                    |
| $Cr^{2+}$ for Mg or $Fe^{2+}$                                   | none  | none                                       |                    |
| Component = $Cr^{2+}SiO_4$                                      | little  | none                                       |                    |
| low   | $M_2\Box M_1^2V^{4+}$                           | $M_2\Box M_1^2V^{4+}$                      |                    |
| $M_2\Box M_1^2V^{3+}$   | $M_2\Box M_1^2V^{3+}$                           | low  |                    |
| none  | $M_2Na - M_1V^{3+}$                             | low  |                    |
| $V^{2+}$ for Mg or $Fe^{2+}$                                    | none  | none                                       |                    |
| $M_2\Box M_1^2Ti^{4+}$  | $M_2\Box M_1^2Ti^{4+}$                          | $M_2\Box M_1^2Ti^{4+}$                     |                    |
| $M_2\Box M_1^2Ti^{3+}$  | none  | none                                       |                    |
| <b>Pyroxene charge balance couples = "others"</b>               |   |  |                    |
| none  | $V^{IV}Fe^{3+} - IVAl$                          | $V^{IV}Fe^{3+} - IVAl$                     |                    |
| none  | $M_2Na - M_1^2Fe^{3+}$                          | $M_2Na - M_1^2Fe^{3+}$                     |                    |
| $M_1Cr^{3+} - IVAl$   | $M_1Cr^{3+} - IVAl$                             | $M_1Cr^{3+} - IVAl$                        |                    |
| none  | $M_2Na - M_1Cr^{3+}$                            | $M_2Na - M_1Cr^{3+}$                       |                    |
| $Cr^{2+}$ for Mg or $Fe^{2+}$                                   | low   | none                                       |                    |
| none  | $M_2Na M_1^2V^{4+} - IVAl$                      | $M_2Na M_1^2V^{4+} - IVAl$                 |                    |
| low   | $M_1V^{4+} - 2IVAl$                             | $M_1V^{4+} - 2IVAl$                        |                    |
| none  | $M_2Na - M_1V^{3+}$                             | low  |                    |
| $M_1V^{3+} - IVAl$  | low   | none                                       |                    |
| $V^{2+}$ for Ca, Mg, $Fe^{2+}$                                  | none  | none                                       |                    |
| $M_1Ti^{3+} - IVAl$   | none  | none                                       |                    |
| $M_1Ti^{4+} - 2IVAl$  | $M_1Ti^{4+} - 2IVAl$                            | $M_1Ti^{4+} - 2IVAl$                       |                    |
| <b>Spinel components</b>  |   |  |                    |
| Moderate  | $IVFe^{3+}(Fe^{3+}Fe^{2+})O_4$ (Magnetite)      | $IVFe^{3+}(Fe^{3+}Fe^{2+})O_4$ (Magnetite) | present            |
|   | (Predicted)                                     |  | present            |
| $IVCr^{2+}V^{IV}Cr^{3+}O_4$                                     | low   | none                                       |                    |
| (Predicted)   | low   | none                                       |                    |
| $(Fe^{2+}, Mg)V^{IV}V^{3+}O_4$ (Coulsonite)                     | low   | none                                       |                    |
| low   | $IVFe^{2+}V^{IV}(Fe^{2+}V^{4+})O_4$ (Predicted) | some                                       |                    |
| $V^{2+}$ for $(Fe^{2+}, Mg)$                                    | none  | none                                       |                    |

lunar olivine contains mostly Cr<sup>2+</sup> whereas coexisting pyroxene contains mostly Cr<sup>3+</sup>. Hanson and Jones (1998) showed that Cr<sup>2+</sup> predominates in basaltic melts at  $f_{O_2}$  less than IW-1. Fe<sup>3+</sup> is very important in Earth, less so in Mars, and almost nonexistent in the Moon. The importance of the Fe<sup>2+</sup> to Fe<sup>3+</sup> transition cannot be overstated, as the crystal-chemical differences, in terms of behavior (based on size and charge), is not unlike the differences between Mg and Al. We note that for pyroxene in six of the seven terrestrial suites that we studied (Papike and White 1979; Papike 1980, 1981), Fe<sup>3+</sup> (in the M1 site) coupled with Al (in the tetrahedral site) is one of the top two most important substitutions. The Fe<sup>3+</sup>-Al substitution is of lesser importance in Mars and is not important in the Moon. The V<sup>3+</sup> to V<sup>4+</sup> transition is important and very useful for olivine oxygen barometry (Canil and Fedortchouk, 2001) because  $D$  for V<sup>3+</sup> is significantly higher than  $D$  for V<sup>4+</sup>. We rationalize this observation in the following way: Most V<sup>3+</sup> and V<sup>4+</sup> substitutions into the olivine structure (other than Na in the M2 site coupled with say V<sup>3+</sup> in the M1 site) involve vacancies, which are quite incompatible in crystal structures. For V<sup>3+</sup>, one vacancy can accommodate two V<sup>3+</sup> cations whereas for V<sup>4+</sup> one vacancy only accommodates one V<sup>4+</sup>. Thus more vacancies are required for V<sup>4+</sup> substitutions into olivine (see discussion above and exchange reactions). In the Moon, V<sup>3+</sup> is much more abundant than V<sup>4+</sup> (Canil 2002; Papike et al. 2004). Thus, in lunar chromite, V<sup>3+</sup> follows Cr<sup>3+</sup>, whereas in Earth V<sup>4+</sup> (which is much greater in abundance than V<sup>3+</sup>) follows Ti<sup>4+</sup> (e.g., in ulvöspinel). We could go on in this vein for some time but we will not. It is much more efficient to present our observations in tabular form (see Table 6).

We note that this review is very different than those we have been involved with in the past. Most reviews are written about a field of study that is mature and may have already “peaked.” However, we are writing about a field “valence-state partitioning over crystallographic sites and phases” that really is in its infancy. It certainly has not reached full bloom! We have done this because we feel strongly that this research direction is very important and we would like more crystal chemists, mineralogists, petrologists, and geochemists to participate. We note that the crystallization sequence, mineral-melt partitioning, nature of fractionation and thus melt evolution for one bulk composition (for example MORB) can be profoundly different over a range of  $f_{O_2}$  from IW-2 to IW + 6. We must better understand the atomistics of valence-state partitioning. What is needed is more experimental work at controlled  $f_{O_2}$ . However, of much more importance is the characterization of the mineral phases with advanced techniques (e.g., XANES) that are capable of not only determining valence states of the element of interest but that can determine which crystallographic sites the valence states are going into. We will also have to understand this process as a function of temperature and pressure.

## ACKNOWLEDGMENTS

This work was funded by a grant to J.P.P. from the NASA Cosmochemistry Program and is in part a contribution to the “Oxygen in the Solar System” initiative of the Lunar and Planetary Institute. This paper was significantly improved by the reviews of K. Righter, M. Rutherford, and editor R. Dymek.

## REFERENCES CITED

- Barnes, S.J. (1986) The distribution of chromium among orthopyroxene, spinel, and silicate liquid at atmospheric pressure. *Geochimica et Cosmochimica Acta*, 50, 1889–1909.
- Beckett, J.R. (1986) The origin of calcium,-aluminum-rich inclusions from carbonaceous chondrites: an experimental study. Ph.D. thesis, University of Chicago, Chicago, Illinois.
- Bence, A.E. (1981) Oceanic intraplate volcanism. In R.B. Merrill and R. Ridings, Eds., *Basaltic Volcanism on the Terrestrial Planets*, p. 161–192. Pergamon, New York.
- Bence, A.E. and Papike, J.J. (1972) Pyroxenes as recorders of lunar basalt petrogenesis: chemical trends due to crystal-liquid interaction. *Proceedings of the 3rd Lunar Science Conference*, 1, 431–469.
- Bence, A.E., Grove, T.L., and Papike, J.J. (1980) Basalts as probes of planetary interiors: constraints on the chemistry and mineralogy of their source regions. *Precambrian Research*, 10, 249–279.
- Bence, A.E., Grove, T.L., Papike, J.J., and Taylor, S.R. (1981) Basalts as probes of planetary interiors: constraints from major and trace element chemistry. In R.B. Merrill and R. Ridings, Eds., *Basaltic Volcanism on the Terrestrial Planets*, p. 311–338. Pergamon, New York.
- Berry, A.J., Shelley, J.G., Foran, G.J., O’Neill, H.S.C., and Scott, D.R. (2003) A furnace design for XANES spectroscopy of silicate melts under controlled oxygen fugacities and temperatures to 1773 K. *Journal of Synchrotron Radiation*, 10, 332–336.
- Burns, R.G., Abu-Eid, R.M., and Huggins, F.E. (1972) Crystal field spectra of lunar pyroxenes. *Proceedings of the 3rd Lunar Science Conference*, 1, 533–543.
- Basaltic Volcanism Study Project (BVSP) (1981) *Basaltic Volcanism on the Terrestrial Planets*. Pergamon, New York 1286 p.
- Cameron, M. and Papike, J.J. (1980) Crystal chemistry of silicate pyroxenes. In C.T. Prewitt, Ed., *Pyroxene*, 7, p. 5–92. *Reviews in Mineralogy*.
- (1981) Structural and chemical variation in pyroxenes. *American Mineralogist*, 66, 1–50.
- Canil, D. (1999) Vanadium partitioning between orthopyroxene, spinel, and silicate melt and the redox states of mantle source regions for primary magmas. *Geochimica et Cosmochimica Acta*, 63, 557–572.
- (2002) Vanadium in peridotites, mantle redox state and tectonic environments: Archean to present. *Earth and Planetary Science Letters*, 195, 75–90.
- Canil, D. and Fedortchouk, Y. (2001) Olivine-liquid partitioning of vanadium and other trace elements, with applications to modern and ancient picrites. *The Canadian Mineralogist*, 39, 319–330.
- Carmichael, I.S.E. and Ghiorso, M.S. (1990) The effect of oxygen fugacity on the redox states of natural liquids and their crystallizing phases. In J. Nicholls and J.K. Russell, Eds., *Modern methods of igneous petrology: understanding magmatic processes*, 24, p. 190–212. *Reviews in Mineralogy*, Mineralogical Society of America, Washington, D.C.
- Connolly, H.C. and Burnett, D.S. (2003) On type B CAI formation: experimental constraints on  $f_{O_2}$  variations in spinel minor element partitioning and re-equilibration effects. *Geochimica et Cosmochimica Acta*, 63, 557–572.
- Consolmagno, G.J. and Drake, M.J. (1977) Composition and evolution of the eucrite parent body. *Geochimica et Cosmochimica Acta*, 41, 1271–1282.
- Delano, J.W. (2001) Redox history of the Earth’s interior since ~3900 Ma: implications for prebiotic molecules. *Origins of Life and Evolution of the Biosphere*, 31, 311–341.
- Drake, M.J., Newsom, H.E., and Capobianco, C.J. (1989) V,Cr, and Mn in the Earth, Moon, EPB, SPB and the origin of the Moon: experimental studies. *Geochimica et Cosmochimica Acta*, 53, 2101–2111.
- Dungan, M.A., Lipman, P.W., and Williams, S. (1981) Continental rift volcanism. In R.B. Merrill and R. Ridings, Eds., *Basaltic Volcanism on the Terrestrial Planets*, p. 108–131. Pergamon, New York.
- Gaetani, G.A. and Grove, T.L. (1996) Partitioning of moderately siderophile elements among olivine, silicate melt, and sulfide melts: constraints on core formation in the Earth and Mars. *Geochimica et Cosmochimica Acta*, 61, 1829–1846.
- Goodrich, C.A. and Delaney, J.S. (2000) Fe/Mg–Fe/Mn relations of meteorites and primary heterogeneity of primitive achondrite parent bodies. *Geochimica et Cosmochimica Acta*, 64, 149–160.
- Goodrich, C.A., Herd, C.D.K. and Taylor, L.A. (2003) Spinel and oxygen fugacity in olivine-phryic and Iherzolitic shergottites. *Meteoritics and Planetary Science*, 38, 1773–1792.
- Green, J.C. and Haskin, L.A. (1981) Pre-Tertiary continental flood basalts. In R.B. Merrill and R. Ridings, Eds., *Basaltic Volcanism on the Terrestrial Planets*, p. 30–77. Pergamon, New York.
- Grove, T.L. and Juster, T.C. (1989) Experimental investigations of low-Ca pyroxene stability and olivine-pyroxene-liquid equilibria at 1 atm in natural basaltic and andesitic liquids. *Contributions to Mineralogy and Petrology*, 103, 287–305.
- Haggerty, S.E. (1972) Apollo 14: subsolidus reduction and compositional variations of spinels. *Proceedings of the 3rd Lunar Science Conference*, 1, 305–322.
- Haggerty, S.E. and Irving, A.J. (1981) Tertiary continental flood basalts. In R.B. Merrill and R. Ridings, Eds., *Basaltic Volcanism on the Terrestrial Planets*, p. 78–107. Pergamon, New York.
- Hanson, B. and Jones, J.H. (1998) The systematics of Cr<sup>3+</sup> and Cr<sup>2+</sup> partitioning between olivine and liquid in the presence of spinel. *American Mineralogist*, 83, 669–684.

- Herd, D.K., Borg, L.E., Jones, J.H., and Papike, J.J. (2002) Oxygen fugacity and geochemical variations in the martian basalts: implications for martian basalt petrogenesis and the oxidation state of the upper mantle of Mars. *Geochimica et Cosmochimica Acta*, 66, 2025–2036.
- Huebner, J.S., Lipin, B.R., and Wiggins, L.B. (1976) Partitioning of chromium between silicate crystals and melts. *Proceedings of the 7<sup>th</sup> Lunar Science Conference*, 1195–1220.
- Jones, J.H. (2004) Redox conditions among the terrestrial planets (abstract). *Lunar and Planetary Science Conference XXXV* 1264. Lunar and Planetary Institute, Houston, (CD-ROM).
- Karner, J.M., Papike, J.J., and Shearer, C.K. (2003) Olivine from planetary basalts: Chemical signatures that indicate planetary parentage and those that record igneous setting and process. *American Mineralogist*, 88, 806–816.
- Karner, J.M., Sutton, S.R., Papike, J.J., Delaney, J.S., Shearer, C.K., Newville, M., Eng, P., Rivers, M., and Dyar, M.D. (2004a) A new oxygen barometer for solar system basaltic glasses based on vanadium valence (abstract). *Lunar and Planetary Science Conference XXXV* 1269. Lunar and Planetary Institute, Houston (CD-ROM).
- Karner, J.M., Papike, J.J., and Shearer, C.K. (2004b) Plagioclase from planetary basalts: Chemical signatures that reflect planetary volatile budgets, oxygen fugacity, and styles of igneous differentiation. *American Mineralogist*, 89, 1101–1109.
- Li, J.-P., O'Neill, H.St. C., and Seifert, F. (1995) Subsolidus phase relations in the system MgO-SiO<sub>2</sub>-Cr-O in equilibrium with metallic Cr, and their significance for the petrochemistry of chromium. *Journal of Petrology*, 36, 107–132.
- Lindstrom, D.J. (1976) Experimental study of partitioning of the transition metals between clinopyroxene and coexisting silicate liquids, Ph.D. thesis. University of Oregon, Eugene, OR.
- McKay, G., Le, L., Schwandt, C., Mikouchi, T., Koizumi, E., and Jones, J.H. (2004) Yamato 980459: the most primitive shergottite? *Lunar and Planetary Science Conference XXXV* 2154. Lunar and Planetary Institute, Houston, (CD-ROM).
- McSween, H.Y. and Treiman, A.H. (1998) Martian meteorites. In J.J. Papike, Ed., *Planetary Materials*, 36, p. 6–1 to 6–53. *Reviews in Mineralogy, Mineralogical Society of America*, Washington, D.C.
- Meyer, C. (2003) Mars Meteorite Compendium-2003. JSC 27672, Revision B, NASA Johnson Space Center, Houston. For updates see <http://www.curator.jsc.nasa.gov/curator/antmet/mmc/mmc.htm>.
- Mikouchi, T., McKay, G., and Le, L. (1994) Cr, Mn, and Ca distributions for olivine in angrite systems: constraints on the origins of Cr-rich and Ca-poor core olivine in angrite LEW87051. *Lunar and Planetary Science*, 25, 907–908.
- Murck, B.W. and Campbell, I.H. (1986) The effects of temperature, oxygen fugacity and melt composition on the behavior of chromium in basic and ultrabasic rocks. *Geochimica et Cosmochimica Acta*, 50, 1871–1887.
- Mysen, B.O. (1987) Magmatic silicate melts: relations between bulk composition, structure and properties. In B.O. Mysen, Ed., *Magmatic processes: physiochemical principles*, p. 375–399. *Geochemical Society, Special Publication No. 1*.
- Naldrett, A.J. and Smith, I.E.M. (1981) Mafic and ultramafic volcanism during the Archean. In R.B. Merrill and R. Ridings, Eds., *Basaltic Volcanism on the Terrestrial Planets* pp. 5–29. Pergamon, New York.
- Papike, J.J. (1980) Pyroxene mineralogy of the Moon and meteorites. In C.T. Prewitt, Ed., *Pyroxenes*, 7, p. 495–525. *Reviews in Mineralogy, Mineralogical Society of America*, Washington D.C.
- (1981) Silicate mineralogy of planetary basalts. In R.B. Merrill and R. Ridings, Eds., *Basaltic Volcanism on the Terrestrial Planets*, pp. 340–363. Pergamon, New York.
- (1987) Chemistry of the rock-forming silicates: ortho, ring, and single-chain structures. *Reviews of Geophysics and Space Physics*, 25, 1483–1526.
- (1996) Pyroxene as a recorder of cumulate formational processes in asteroids, Moon, Mars, Earth: reading the record with the ion microprobe. *American Mineralogist*, 81, 525–544.
- (1998) Comparative planetary mineralogy: chemistry of melt-derived pyroxene, feldspar, and olivine. In J.J. Papike, Ed., *Planetary Materials*, Volume 36, p. 7–01 to 7–10. *Reviews in Mineralogy, Mineralogical Society of America*, Washington D.C.
- Papike, J.J. and Bence, A.E. (1978) Lunar mare versus terrestrial mid-ocean ridge basalts: planetary constraints on basaltic volcanism. *Geophysical Research Letters*, 5, 803–806.
- Papike, J.J. and Cameron, M. (1976) Crystal chemistry of silicate minerals of geophysical interest. *Reviews of Geophysics and Space Physics*, 14, 37–80.
- Papike, J.J. and White, C. (1979) Pyroxenes from planetary basalts: characterization of “other” than quadrilateral components. *Geophysical Research Letters*, 6, 913–916.
- Papike, J.J., Hodges, F.N., Bence, A.E., Cameron, M., and Rhodes, J.M. (1976) Mare basalts: crystal chemistry, mineralogy, and petrology. *Reviews of Geophysics and Space Physics*, 14, 475–540.
- Papike, J.J., Fowler, G.W., Shearer, C.K., and Layne, G.D. (1996) Ion microprobe investigation of plagioclase and orthopyroxene from lunar Mg-suite norites: implications for calculating parental melt REE concentrations and for assessing postcrystallization REE redistribution. *Geochimica et Cosmochimica Acta*, 60, 3967–3978.
- Papike, J.J., Shearer, C.K., and Ryder, G. (1998) Lunar samples. In J.J. Papike, Ed., *Planetary Materials*, 36, p. 5–1 to 5–234. *Reviews in Mineralogy, Mineralogical Society of America*, Washington D.C.
- Papike, J.J., Fowler, G.W., Adcock, C.T., and Shearer, C.K. (1999) Systematics of Ni and Co in olivine from planetary melt systems: lunar mare basalts. *American Mineralogist*, 84, 392–399.
- Papike, J.J., Karner, J.M., and Shearer, C.K. (2004) Comparative planetary mineralogy: V/(Cr + Al) systematics in chromite as an indicator of relative oxygen fugacity. *American Mineralogist*, 89, 1557–1560.
- Pearce, J.A., Barker, P.F., Edwards, S.J., Parkinson, I.J., and Leat, P.T. (2000) Geochemistry and tectonic significance of peridotites from South Sandwich arc-basin, South Atlantic. *Contributions to Mineralogy and Petrology*, 139, 36–53.
- Rhodes, J.M. and Bence, A.E. (1981) Ocean floor basaltic volcanism. In R.B. Merrill and R. Ridings, Eds., *Basaltic Volcanism on the Terrestrial Planets*, pp. 132–160. Pergamon, New York.
- Righter, K., Sutton, S.R., and Newville, M. (2004) Micro-XANES measurements on experimental spinels and the oxidation state of vanadium in spinel-melt pairs. (abstract). Oxygen in the Terrestrial Planets workshop, 3010. *Lunar and Planetary Institute*, Houston (CD-ROM).
- Schreiber, H.D. (1977) Redox states of Ti, Zr, Hf, Cr, and Eu in basaltic magmas: an experimental study. *Proceedings of 8<sup>th</sup> Lunar Science Conference*, 1785–1807.
- (1987) An electrochemical series of redox couples in silicate melts: a review and applications to geochemistry. *Journal of Geophysical Research*, 92, 9225–9232.
- Schreiber, H.D. and Haskin, L.A. (1976) Chromium in basalts: Experimental determination of redox states and partitioning among silicate phases. *Proceedings of the 7<sup>th</sup> Lunar Science Conference*, 513–538.
- Schreiber, H.D., Merkel, R.C., Schreiber, V.L., and Balazs, G.B. (1987) Mutual interactions of redox couples via electron exchange in silicate melts: models for geochemical melt systems. *Journal of Geophysical Research*, 92, 9233–9245.
- Shannon, R.D. and Prewitt, C.T. (1969) Effective ionic radii in oxides and fluorides. *Acta Crystal*, B25, 925–946.
- Shervais, J.W. (1982) Ti-V plots and the petrogenesis of modern and ophiolitic lavas. *Earth and Planetary Science Letters*, 59, 101–118.
- Stolper, E. (1979) Trace elements in shergottite meteorites: implications for the origins of planets. *Earth and Planetary Science Letters*, 42, 239–242.
- Sutton, S.R., Jones, K.W., Gordon, B., Rivers, M.L., Bajt, S., and Smith, J.V. (1993) Reduced chromium in olivine grains from lunar basalt 15555: X-ray absorption near edge structure (XANES). *Geochimica et Cosmochimica Acta*, 57, 461–468.
- Sutton, S.R., Simon, S.A., Grossman, L., Delaney, J.S., Beckett, J., Newville, M., Eng, P., Rivers, M., and Dyar, M.D. (2002) Evidence for divalent vanadium in Allende CAI fassaite and implications for formation conditions (abstract). *Lunar and Planetary Science Conference XXXIII* 1907. *Lunar and Planetary Institute*, Houston (CD-ROM).
- Sutton, S.R., Karner, J.M., Papike, J.J., Delaney, J.S., Shearer, C.K., Newville, M., Eng, P., Rivers, M., and Dyar, M.D. (2005) Vanadium K Edge XANES of Synthetic and Natural Basaltic Glasses and Application to Microscale Oxygen Barometry. *Geochimica et Cosmochimica Acta*, in press.
- Taylor, S.R., Arculus, R., Perfit, M.R., and Johnson, R.W. (1981) Island arc basalts. In R.B. Merrill and R. Ridings, Eds., *Basaltic Volcanism on the Terrestrial Planets*, pp. 193–213. Pergamon, New York.
- Toplis, M.J. and Corgne, A. (2002) An experimental study of element partitioning between magnetite, clinopyroxene and iron-bearing silicate liquids with particular emphasis on vanadium. *Contributions to Mineralogy and Petrology*, 144, 22–37.
- Wadhwa, M. (2001) Redox state of Mars' upper mantle and crust from Eu anomalies in shergottite pyroxenes. *Science*, 291, 1527–1530.
- Waychunas, G.A. (1991) Crystal chemistry of oxides and oxyhydroxides. In D.H. Lindsley, Ed., *Oxide minerals: petrologic and magnetic significance*, 25, 11–68. *Reviews in Mineralogy, Mineralogical Society of America*, Washington D.C.
- Wechsler, B.A., Lindsley, D.H., and Prewitt, C.T. (1984) Crystal structure and cation distribution in titanomagnetites ( $Fe_{3-x}Ti_xO_4$ ). *American Mineralogist*, 69, 754–770.
- Wright, T.L. and Okamura, R.T. (1977) Cooling and crystallization of tholeiitic basalt, 1965 Makaopuhi Lava Lake, Hawaii, Geological Survey Professional Paper 1004, U.S. Government Printing Office, Washington. 78 pp.
- Zolensky, M.E., Pieters, C., Clark, B., and Papike, J.J. (2000) Small is beautiful: the analysis of nanogram-sized astromaterials. *Meteoritics & Planetary Science*, 35, 9–29.

MANUSCRIPT RECEIVED JULY 30, 2004

MANUSCRIPT ACCEPTED OCTOBER 31, 2004

MANUSCRIPT HANDLED BY ROBERT F. DYMELK